AFRPL-TR-81-27

COLLISIONAL EXCITATION OF H_2O AND CO_2 BY $O(^3P)$ ATOMS.

Final technical rpt. 1 Oct 79—11 Sep 80.

Rodney J. Bartlett
Michael J. Redmon

BATTELLE COLUMBUS LABORATORIES
505 KING AVENUE
COLUMBUS, OH 43201

FEB 81

F04611-79-C-0054

AIR FORCE ROCKET PROPULSION LABORATORY
DIRECTOR OF SCIENCE AND TECHNOLOGY
AIR FORCE SYSTEMS COMMAND
EDWARDS AFB, CALIFORNIA 93523

FOREWORD

PATRICK M. SAATZER, Capt. USAF
Project Manager

DAVID MANN
Chief, Plume Technology Branch

FOR THE COMMANDER

EUGENE G. HABERMAN
Chief, Propulsion Analysis Division

REPORT DOCUMENTATION PAGE	READ INSTRUCTIONS BEFORE COMPLETING FORM

1 REPORT NUMBER AFRPL-TR-81-27	2 GOVT ACCESSION NO. AD-A101184	3 RECIPIENT'S CATALOG NUMBER

4. TITLE (and Subtitle) COLLISIONAL EXCITATION OF H_2O AND CO_2 BY O(3P) ATOMS	5. TYPE OF REPORT & PERIOD COVERED FINAL TECHNICAL- June 11 through September 11, 1980
	6 PERFORMING ORG. REPORT NUMBER

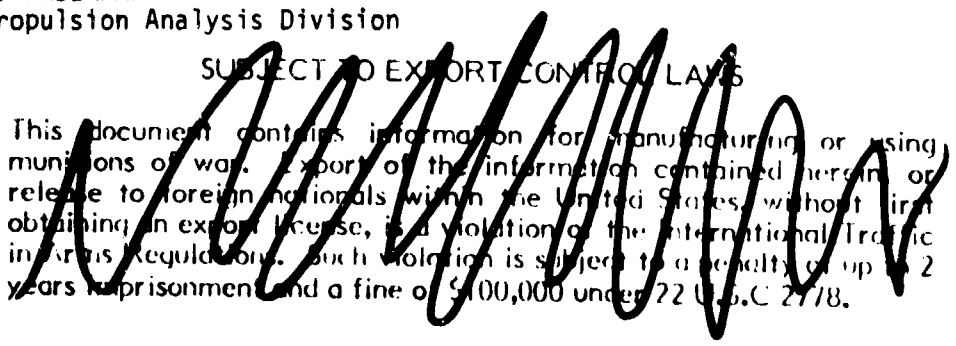| 7 AUTHOR(s) Rodney J. Bartlett Michael J. Redmon	8. CONTRACT OR GRANT NUMBER(s) F04611-79-C-0024

9 PERFORMING ORGANIZATION NAME AND ADDRESS BATTELLE COLUMBUS LABORATORIES 505 KING AVENUE COLUMBUS OHIO 43201	10. PROGRAM ELEMENT, PROJECT, TASK AREA & WORK UNIT NUMBERS

11. CONTROLLING OFFICE NAME AND ADDRESS AIR FORCE ROCKET PROPULSION LABORATORY EDWARDS AIR FORCE BASE CALIFORNIA 93523	12. REPORT DATE February 1981
	13. NUMBER OF PAGES 104

14 MONITORING AGENCY NAME & ADDRESS(if different from Controlling Office)	15. SECURITY CLASS. (of this report) UNCLASSIFIED
	15a. DECLASSIFICATION/DOWNGRADING SCHEDULE

16. DISTRIBUTION STATEMENT (of this Report)

Approved for public release: Distribution unlimited

17. DISTRIBUTION STATEMENT (of the abstract entered in Block 20, if different from Report)

Approved for public release: Distribution unlimited

18. SUPPLEMENTARY NOTES

19. KEY WORDS (Continue on reverse side if necessary and identify by block number)

Vibrational Excitation Cross Sections   Quasiclassical Collision Dynamics
Collisionally Induced Infrared Radiation
Vibrational Rotational Infrared Radiation
Cross Sections $H_2O + O$, $CO_2 + O$
Potential Energy Surface

20. ABSTRACT (Continue on reverse side if necessary and identify by block number)

Theoretical calculations of the molecular excitation cross sections for: $O(^3P) + H_2O(^1A_1)$ and $O(^3P) + CO_2 (^1\Sigma g^+)$ collisions were made as a function of velocity over the range 2 - 10km/sec. Potential surfaces for these reactions were computed using the many body perturbation technique. Trajectory calculations were performed with a monte carlo quasi-classical trajectory technique. To obtain an accurate analytical fit of the potential surface a many body force field was employed. Also to obtain good action angle variables a technique was developed to perform final state analysis. The results for H_2O are insensitive to within a factor of 2 for substantial changes in the fit parameters. This

DD FORM 1473 EDITION OF 1 NOV 65 IS OBSOLETE
1 JAN 73

20.

provides a measureable degree of confidence of the predicted results. Representative values for H_2O (001) + 0 are 2.0 x 10^{-17} cm^2 at 4km/sec and 2.0 x 10^{-16} cm^2 at 6km/sec. The results for CO_2 + 0 are not as reliable due to the use of a simplier fit of the surface. The results for CO_2 show that excitation of NN'I states is more probable by up to two orders of magnitude than direct excitation of the 001 state. If radiation from the 001 state is observed then a multiple collision environment probably exists. Representative values for CO_2 (001) + 0 are 3.0 x 10^{-19} cm^2 at 6km/sec and 2.5 x 10^{-18} cm^2 at 8km/sec.

10 to the minus 19th power.

10 to the minus 6th power

10 to the minus 17th power 6 cm

10 to the minus 18th power

TABLE OF CONTENTS

Accession For

NTIS GRA&I	☒
DTIC TAB	☐
Unannounced	☐
Justification_____	

By_____
Distribution/
Availability Codes

| Dist | Avail and/or Special |

A

1

Page

LIST OF TABLES
(Continued)

LIST OF FIGURES

Page

LIST OF FIGURES
(Continued)

EXECUTIVE SUMMARY

A principal component for the design of future surveillance systems is a detailed description of rocket plume characteristics. This description of plumes is primarily built upon state-to-state excitation cross sections for certain very specific collision processes. These processes, predominantly involving atomic oxygen and plume exhaust gases, are now believed to be the crucial driving mechanisms for the enhanced intensity of infra-red radiation from plumes at altitudes above 100-200 kilometers. Such cross sections are requisite input to sophisticated hydrodynamic plume modeling codes, which require kinetic information for as many as one hundred different microscopic molecular processes.

For many of these kinetic processes, the required information is not available from experiment. In other cases, the experimental methods have proven expensive, and sometimes unreliable. It is felt that the sophisticated methods of modern theoretical chemistry can often provide a cost-effective means for predicting state-to-state cross sections caused by collisions in plumes. Theoretical calculations also assist in the interpretation of the experimental results.

The intent of this project is to use current, state-of-the-art _ab_ _initio_ theoretical chemistry computations to predict a series of cross sections for vibrational excitations caused by $O(^3P)$ atoms colliding with the two plume species, H_2O and CO_2. These studies are the first results for systems of this complexity, determined at the degree of sophistication employed in this investigation. All calculations are "first-principle",

7

meaning they are built solely upon the laws of physics and quantum mechanics. Only a knowledge of the atoms and molecules involved in the collision is required information. There is no scaling to experimental values, no adjustable parameters, and no attempt to use crude, often structureless, models for the collisions. Furthermore, most of the results reported here have been obtained prior to any experimental information.

In the collision of $O(^3P)$ with $H_2O(^1A_1)$, results are reported for the vibrational excitation cross sections, (001), (100), (010), (011), (110), (200), (020), and (002), at a collisional velocity range above 4 km/sec. For CO_2, the cross sections (001), (100), (010), (020), (110), (030) over a velocity range of 6-10 km/sec are given.

The report describes the three steps in the calculation, the ab initio computation of points on the potential energy surface for the collision, the method of making an analytic fit to the computed points, and the details of the cross section determination by quasiclassical trajectory methods. Emphasis is placed on the possible errors that can occur, and the justification for the reliability of the results. Several recommendations for future work are offered.

I. INTRODUCTION

Above 100-200 kilometers, rocket exhaust plumes show a
significantly increased level of in .ared emission compared to what
would be expected based upon assumptions of local thermodynamic
equilibrium[1,2] A large and diverse data base obtained by field
observations and laboratory experiments, assisted by gas-dynamical models
of the upper atmosphere, have explained this increased infrared
emission by a series of basic physical mechanisms.[1,2] One of these
important mechanisms involves collisions among atomic oxygen, the
dominant lower ionosphere species, and plume exhaust gases such as CO_2,
H_2O, HF, and F .i. These collisions cause an increase in the population
of excited, infrared active vibrational-rotational states for the
molecules in the exhaust gas, which then emit radiation in the infrared.

However, in spite of our understanding of the basic physical
mechanisms underlying the observed phenomena, there is little
detailed signature data for low-thrust/low-intensity targets. This lack
of information has made the design of future surveillance systems quite
difficult.[1,2]

As an alternative to a knowledge of detailed signature data,
high-altitude target prediction computer models have been used to
determine the infrared intensity levels. These computational models
employ fluid mechanics for nonlocal thermodynamic equilibrium environments,
and among other things, must incorporate data for nonequilibrium
molecular radiation phenomena.[2,3] Consequently, these high-altitude

9

signature codes are based upon detailed information about the inelastic
energy transfer processes that occur in hyperthermal collisions.
Specifically, it is necessary to know the probability that a molecule
will undergo a particular vibrational-rotational transition when colliding
with atomic oxygen. These probabilities are referred to as "cross-
sections," and these cross-sections are required input to the computer
models of plume radiation.

In the absence of experimental determinations of such cross
sections, it has been necessary to rely upon estimated and probably
unrealistic values for these quantities. This is the most serious
limitation of the high-altitude plume signature models. Consequently,
a substantial effort toward resolving this problem by obtaining
reliable values for these inelastic cross sections is of high priority.

Cross sections may be obtained in principle by shock-tube and
crossed-molecular beam experiments.[4] However, such experiments are
difficult to perform and to interpret. It is also possible to predict
cross sections from first-principle theoretical calculations.
This is the intent of the present project.

The contribution of accurate theoretical calculations
to the problem of vibrational excitation cross sections is three-fold:

(1) Strong theoretical support is required to assist in
    interpreting the experimental data

(2) Theoretical calculations will often be the only way
    to predict cross sections not presently accessible
    to experimental techniques

10

(3) The reliability of molecular calculations has pro-
gressed sufficiently in recent years that one can
anticipate that _ab_ _initio_ theoretical calcula-
tions can predict accurate values for inelastic
vibrational cross sections in many cases.

If such theoretical calculations are found to be accurate to within
a required tolerance (nominally a factor of 2), then the calculations
may become the most cost effective approach to providing the
requisite cross sections.

In the following, we report on the accurate, first-principle
predictions of the vibrational excitation cross sections for the reactions

$$O(^3P) + H_2O(ooo) \rightarrow H_2O(\nu_1 \nu_1 \nu_3) + O(^3P) \qquad (1)$$

and

$$O(^3P) + CO_2(ooo) \rightarrow CO_2(\nu_1 \nu_2 \nu_3) + O(^3P) \quad . \qquad (2)$$
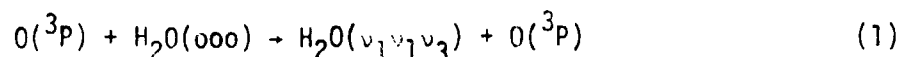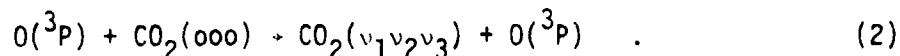
These calculations employ techniques that are state-of-the art for
inelastic collisions of this complexity. Furthermore, with the exception
of a single shock-tube result for a cross section in H_2O near threshold
that dates back to 1975,[5] all results reported here were obtained prior
to any experimental information on these two collision systems. As such,
this effort represents something of a milestone in the application of
first-principle theoretical calculations to the problem of
immediate importance to the national defense.

The theoretical approach to the prediction of cross sections has three parts:

(1) Prediction of the Potential Energy Surface (PES) for the collision.

(2) Analytic fit to the PES.

(3) Quasiclassical trajectory calculations to obtain the cross sections.

In order to obtain high accuracy in the predicted cross sections, it is necessary to maintain a high standard of reliability in each phase of this study. Section II provides a synopsis of many-body perturbation theory (MBPT),[6,7] which is the ab initio method used to generate points on the PES. This is followed by Section III, a detailed discussion of the $O(^3P) + H_2O(^1A_1)$ cross sections, subdivided into four components, the PES, the analytic fit, a discussion of the quasiclassical trajectory method, and the actual determination of the vibrational excitation cross-sections. Section IV reports on the $O(^3P) + CO_2(^1\Sigma_g^+)$ cross sections, also divided into four parts. The final section, V, summarizes the project, evaluates the accuracy of the calculations, and provides suggestions for further work.

II. A SYNOPSIS OF MANY-BODY PERTURBATION THEORY

The calculation of several points on a PES requires accurate and efficient ab initio methods that properly include the effects of electron correlation. This work employs MBPT built upon an unrestricted Hartree-Fock (UHF) reference function for this purpose.[6] Although comparatively new in applications to potential energy surfaces, MBPT offers a number of features that recommend its development for this type of problem.

These features include "size-extensivity" or the correct scaling of the calculation with molecular size.[6,7] This is important in extensions to larger molecules and in predicting the correct dissociation energies when comparing a molecule and its fragments.[7-12] A truncated configuration interaction (CI) calculation is not size-extensive, although "full CI" (including all excitations) and certain other models like generalized valence bond (GVB) are. Also, unlike CI, MBPT permits the inclusion of quadruple and higher CI excitations in convenient, tractable ways which also serves to enhance the comparative efficiency of MBPT over CI.

There are also disadvantages, largely due to the present practical limitation to single reference functions. (The multireference function MBPT theories exist,[13,14] but have not yet been implemented in general purpose codes.) A restriction to a single reference function usually requires that an unrestricted Hartree-Fock (UHF) function be used to study open-shell systems. This has the effect that for some

13

cases, large degrees of spin-contamination can remain in the calculations $[N_2(^1\Sigma_g^+)$ is a case in point, where UHF is used to obtain correct separation to $N(^4S)$ atoms[6]], although for many genuine open-shells this is not a problem [e.g., $O(^3P)$, $N(^4S)$, $HCO(^2A')$][6] In the present calculations, the multiplicity of the $O(^3P) + H_2O(^1A_1)$ and $O(^3P) + CO_2(^1\Sigma_g^+)$ surfaces are monitored and found to always be better than 3.01, so the UHF starting point does not suffer in this application from excessive spin contamination. Also, only the lowest state of a given symmetry can normally be obtained from the single-reference function approach. We will return to this last point in the discussion of the $O(^3P) + H_2O(^1A_1)$ surfaces.

Assuming a self-consistent field (SCF) starting point, the defining equations of MBPT are

$$H_0 = \sum_i^n [h(i) + u(i)] \tag{1}$$

$$V = \sum_{i<j}^n r_{ij}^{-1} - \sum_i^n u(i) \tag{2}$$

$$H_0\phi_0 = E_0\phi_0 \tag{3}$$

$$E_0 = \sum_i^n \varepsilon_i \tag{4}$$

$$\phi_0 = A(x_1(1)x_2(2)\ldots x_n(n)) \tag{5}$$

$$E = E_0 + \sum_{p=0}^{\infty} \langle \phi_0|V[(E_0-H_0)^{-1}V]^p|\phi_0\rangle_L \quad . \tag{6}$$

14

The unperturbed hamiltonian, H_0, consists of the usual one-electron
hamiltonian and the SCF effective one-particle potential. ψ_0 is the SCF
function composed of the occupied orbitals $\{x_i\}$ associated with the
orbital energies $\{\epsilon_i\}$. The linked diagram theorem, Eq. (6), defines the
energy as a sum of diagrams where the subscript L restricts them to "linked"
diagrams. Each diagram provides an algebraic expression in terms of the
transformed two-electron integrals, $\langle x_p x_q || x_r x_s \rangle = \langle pq || rs \rangle = (x_p x_r | x_q x_s)$
$- (x_p x_s | x_q x_r)$, and the orbital energies $\{\epsilon_i\}$. By simply evaluating these
expressions composed solely of information generated in the SCF calculations,
the correlation contributions, E_n, for $n \geq 2$ are obtained. This is a very
efficient process leading to easily vectorizable codes that are ideally
suited to the new generation of computers.

As an example, in second-order

$$E_2 = \sum_{\substack{i > j \\ a > b}} | \langle ij || ab \rangle |^2 / (\epsilon_i + \epsilon_j - \epsilon_a - \epsilon_b) \tag{7}$$

where i, j are orbitals occupied in ψ_0 and a, b are excited SCF orbitals.
This term, which takes a negligible amount of time in addition to the
SCF calculation, accounts for the bulk of the correlation effects in
a problem. However, we have found that to get very good relative energy
differences at adjacent points it is usually necessary to include E_3 and
most of E_4.[6,7] The latter model, SDQ-MBPT(4), refers to all single, double,
and quadruple excitation effects through fourth-order. This model does
neglect the triple excitations, but their inclusion would excessively
increase the required computer time for what appears to be little

15

additional benefit. In comparisons with the infinite-order coupled-cluster doubles model, one seldom finds more than 1 kcal/mole difference due to the higher than fourth-order contributions,[6] so this model is highly stable with respect to possible higher-order corrections of the same type as those included in fourth-order.[7]

A number of applications have shown that calculations at the SDQ-MBPT(4) level and with at least a double-zeta plus polarization basis set are capable of predicting the binding energies in the reactions $2BH_3 \rightarrow B_2H_6$, $BH_3 + CO \rightarrow H_3BCO$, and $BH_3 + NH_3 \rightarrow H_3BNH_3$ to within ± 2 kcal/mole.[10] Similarly, the activation barriers and the isomerization energies of the unimolecular isomerization reactions $CH_3NC \rightarrow CH_3CN$ and $HNC \rightarrow HCN$[11] are exceptionally accurate. In applications to the potential energy surface for the reaction $HCO \rightarrow H + CO$,[12] the quartic force field of H_2O,[8] and the step-wise decomposition of methanol,[9] it is shown that methods at this level are reliable for determining bond lengths and bond angles, and in the case of H_2O, for calculating force-constants even including the higher-order anharmonic constants. One therefore has every reason to expect that the SDQ-MBPT(4) model with an adequate basis set should provide an accurate description of the ground state triplet surface.

III. $O(^3P)$ + $H_2O(^1A_1)$ COLLISION

A. Potential Energy Surface

Before considering the global aspects of the $O(^3P)$ + $H_2O(^1A_1)$
surface, it is pertinent to focus on the two individual fragments. The
SCF and correlation energies for a range of basis sets are presented in
Table I.

The (5s4p2d/3s1p) Slater orbital (STO) basis has been used
in a study of the quartic force field of H_2O.[8] These calculations
are done using SCF, SD-CI, and with various many-body models. The
theoretical results agree well with the experimental force constants,
with the many-body values showing better agreement than SD-CI. In fact,
the most recent experimental and normal coordinate study revises several
of the previously accepted force constants to be more consistent with
these theoretical calculations.[8] All of the cubic and quartic constants
are determined from the calculations, while the experimental studies
typically set many of these constants to zero to facilitate obtaining
the force field from the normal coordinate analysis. Hence, the
computed SDQ-MBPT(4) quartic force field for H_2O is used as input to
the local description of H_2O in the O + H_2O surface fit. This is described
in detail in Section III.B.

Since it would be very expensive to use a STO basis for the
four atom surface calculations, a double-zeta plus polarization (DZP)
contracted Gaussian basis is used to determine the behavior of the surface
describing the approach of the oxygen atom to the H_2O molecule. The
results in this basis are compared for H_2O to the STO basis and other
contracted Gaussian bases[8] in Table I. In the case of the DZP results,

17

TABLE 1. ENERGIES FOR O(^{3}P) AND H$_2$O(^{1}A$_1$), AND GEOMETRIES FOR H$_2$O(^{1}A$_1$) IN DIFFERENT BASIS SETS. ALL ENERGIES ARE IN HARTREE A.U. AND DISTANCES IN BOHRS

	O(^{3}P)		H$_2$O(^{1}A$_1$)			
	(4s2p1d)CGTO[a]	(5s3p1d)CGTO	(4s2p/2s)CGTO	(4s2p1d/2s1p)CGTO[a]	(5s3p1d/3s1p)CGTO	(5s4p2d/3s1p)STO[c]
E_{SCF}	-74.8056	-74.8070	-76.0093	-76.0466	-76.0473	-76.0642
(Estimated SCF limit)		(-74.8120)[b]				(-76.0675)[c]
E_2	-0.0985[a]	-0.1355	-0.1378	-0.2019[a]	-0.2411	-0.2818
E_3	-0.0128[a]	-0.0100	-0.0021	-0.0059[a]	-0.0037	-0.0032
E_4(SDQ)	-0.0018[a]	-0.0140	-0.0047	-0.0025[a]	-0.0032	-0.0031
E_{corr}	-0.1131[a]	-0.1466	-0.1446	-0.2103[a]	-0.2480	-0.2881
(E_{corr}[Exp])		(-0.245)[e]				(-0.370)[c]
E_{corr}(valence)	-0.1131	-0.1274	-0.1309	-0.2103	-0.2297	-0.2462
(E_{corr}(valence)[Exp])		(-0.186)[e,d]				(00.366)[-,d]
2S+1	3.001	3.001	1.000	1.000	1.000	1.000
R_{OH}[SDQ-MBPT(4)]				1.8139		1.8081
(R_{OH}[Exp])						(1.810[f], 1.809[g])
θ_{HOH}[SDQ-MBPT(4)]				104.38°		104.62°
(θ_{HOH}[Exp])						(104.48[f], 104.52[g])
ΔE[H$_2$O(linear)-H$_2$O(Eq.)]				0.055 (1.50eV)		
Separated Limit				-151.17567		

18

[a] The double-zeta plus polarization basis are those used in the complete surface study of the $O(^3P) + H_2O(^1A_1)$ surface. All calculations are done by freezing the $1s^2$ core in the oxygen atoms at the SCF level. Hence, the correlation energies reported in this case are solely for the valence electrons.

[b] P. S. Bagus, B. Liu, and H. F. Schaefer, III, Phys. Rev. A2, 555 (1970).

[c] R. J. Bartlett, I. Shavitt, and G. D. Purvis, J. Chem. Phys. 71, 281 (1979).

[d] Valence shell correlation energies are obtained from the experimental values by subtracting the KK, and KL shell contributions to the correlation energy obtained by R. K. Nesbet, Phys. Rev. 175, 2 (1961), for the He isoelectronic sequence.

[e] J. A. Pople and J. S. Binkley, Mol. Phys. 29, 599 (1975).

[f] A. R. Hoy and P. R. Bunker, J. Mol. Spectrosc. 74, 1 (1979).

[g] A. R. Hoy, I. M. Mills, and G. Strey, Mol. Phys. 24, 1265 (1972).

the oxygen 1s electrons are kept frozen at the SCF level, so only the valence correlation energy is computed. The other results are modified to provide a valence correlation result for comparison.

Although the best H_2O calculation provides about 80% of the valence correlation energy the DZP basis still gives 69%. In addition, the bond length and bond angle in this basis differ only slightly from the STO calculation. These results suggest that we should adequately describe the shape of the surface at this level. In fact, as will be seen below, the $O + H_2O$ triplet surfaces are sufficiently simple, that even a DZ basis would not lead to much of an error in the surface. For the oxygen atom, the DZP basis accounts for 61% of the valence correlation energy, leading to a separated limit of -151.17567 a.u. One additional piece of information provided in Table 1 is the barrier to inversion for H_2O. This is found to be 1.5eV by optimizing the nonlinear and linear H_2O structures. Since for collision energies of 0.5 to 2.5 eV inversion can occur, the cross-sections will be sensitive to the possibility of inversion in the bending mode.

The collision between $O(^3P)$ atoms and ground state H_2O results in three electronic surfaces that correlate with $O(^3P)$. These are illustrated in the correlation diagram in Figure 1, for different directions of approach of the oxygen atom. The one pertinent reaction channel giving $2OH(^2\pi)$ molecules is also indicated. The primary objective of the present work is to investigate the lowest of these surfaces. Since all three surfaces are relevant to a description of the collision dynamics, the higher two surfaces will be considered to some degree.

20

Approach on C_2 Axis (C_{2v} Symmetry)

Off-Axis Approach in Plane of H_2O (C_s Symmetry)
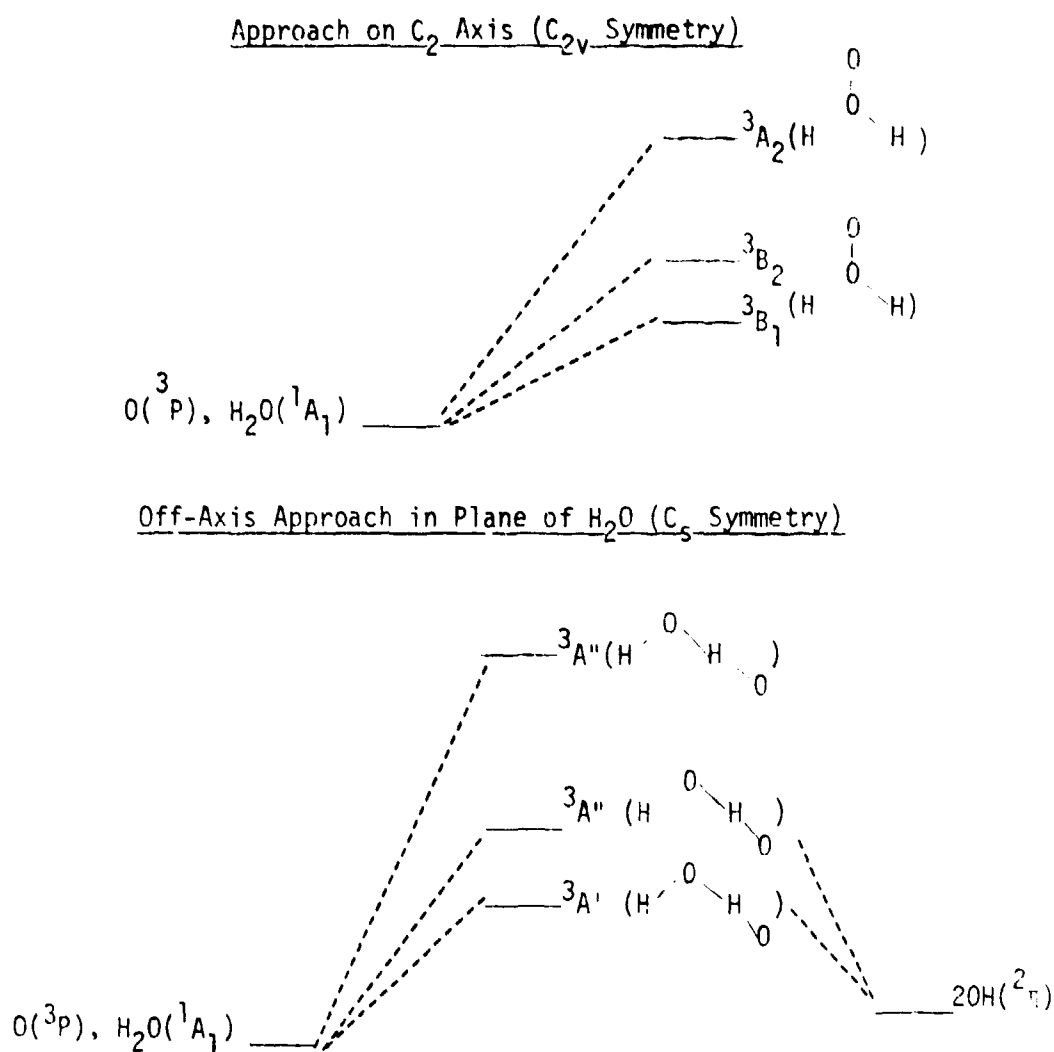
Depending upon the symmetry involved when $O(^3P)$ approaches H_2O, the three electronic states may all be of different symmetries, two different symmetries, or all of the same symmetry. As long as the symmetries are different, the UHF-MBPT approach can be used to obtain the surface. However, it cannot conveniently calculate an excited surface of the same symmetry as a lower state, since the UHF solution is difficult to obtain and may suffer from large amounts of spin contamination.

If H_2O is placed in the yz plane, such that the z-axis corresponds to the two-fold rotation axis, as in Figure 2, different approaches may be considered. An approach of the colliding atom in the yz plane along the molecular axis maintains the C_{2v} symmetry of the system. For this approach it is possible to obtain $^3B_1$, $^3B_2$, and $^3A_2$ surfaces. Similarly, an approach maintaining a single plane of symmetry, such as along the y-axis but in the plane of the molecule, results in C_s symmetry with one A' and two A" states. If there is no plane of symmetry, only the single lowest state is obtained. Figure 2 shows the distribution of ab initio calculations for H_2O at equilibrium. Also calculations using various displacements of H_2O are used. To date, more than 90 points on the various surfaces have been computed. Some of these are listed in Tables 2-9.

Figures 3-7 show curves describing different cuts through the triplet surfaces. It is apparent from all of the figures that these are essentially repulsive, at least for small O-H bond displacements. This should be contrasted with a surface describing the interaction between H_2O and a singlet oxygen atom which would have a number of local extrema including the three minima in the H_2O_2 (hydrogen proxide) structure.

22
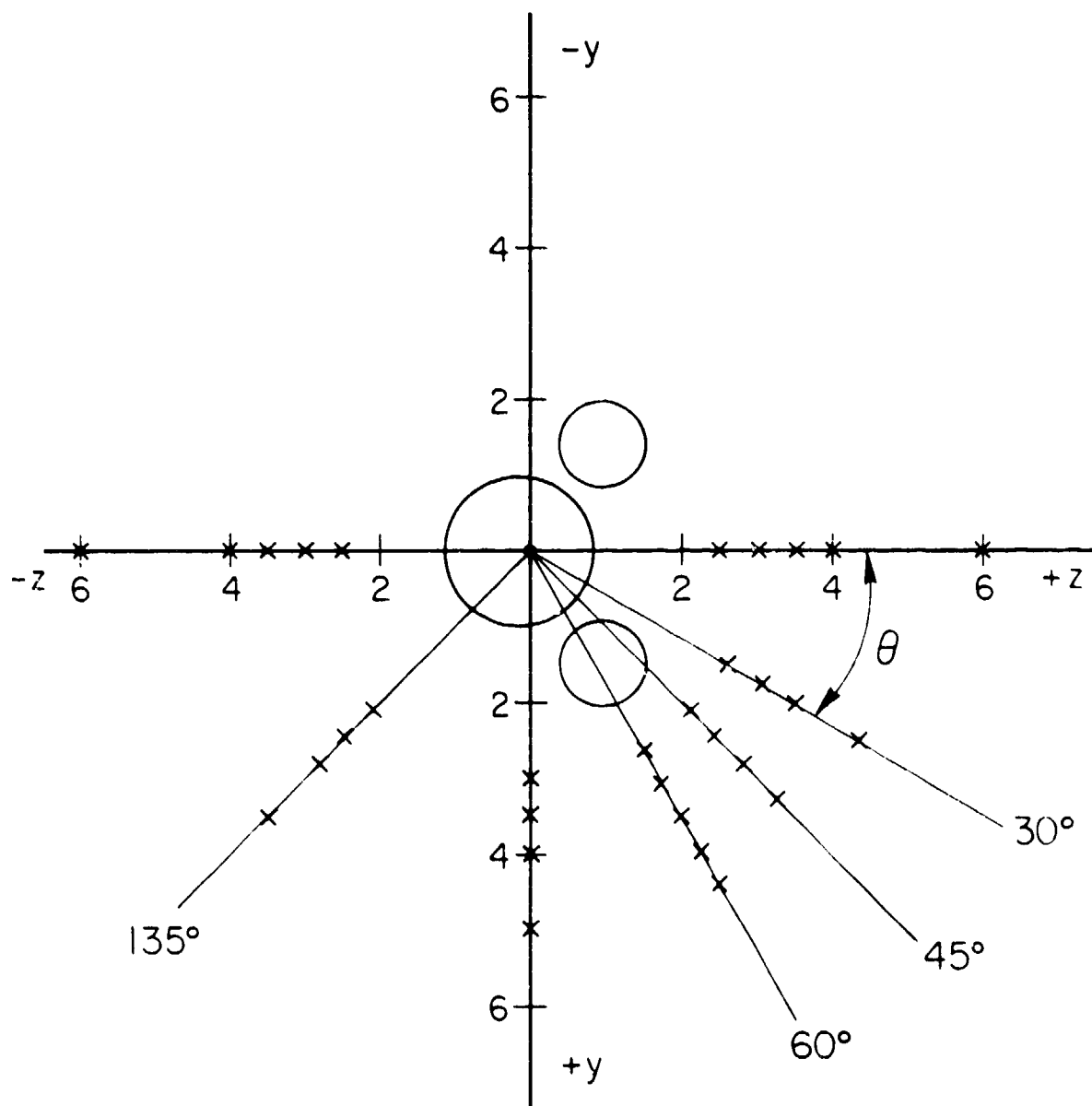
FIGURE 2.   DISTRIBUTION OF AB INITIO POINTS IN THE H_2O PLANE
FOR EQUILIBRIUM H_2O

TABLE 2. H_2O AT EQUILIBRIUM.[a] COLLIDING O-ATOM APPROACHING ALONG THE NEGATIVE Z-AXIS

Distance to O Atom(bohr)[b]	SCF	SDQ-MBPT(4)
$^3B_1$ Ground State		
-2.5	-150.56647	-150.93642
-3.0	-150.72168	-151.06774
-4.0	-150.83686	-151.16515
-6.0	-150.85317	-151.17711
-8.0	-150.85259	-151.17621
$^3B_2$ First Excited State		
-2.5	-150.52779	-150.88583
-3.0	-150.70554	-151.04874
-4.0	-150.83389	-151.16192
-6.0	-150.85288	-151.17682
-8.0	-150.85253	-151.17615
$^3A_2$ Second Excited State		
-2.5	-150.28980	-150.64314
-3.0	-150.57280	-150.91766
-4.0	-150.80587	-151.13298
-6.0	-150.84993	-151.17386
-8.0	-150.85171	-151.17530

[a] Coordinates of H_2O molecule in bohrs are (O :0.0,0.0,-0.12371;H:0.0,$\pm$1.43085, 0.98168). Total energies in Hartrees.

[b] Distance is measured from the center-of-mass of the H_2O molecule.

24

TABLE 3. H_2O AT EQUILIBRIUM.[a] COLLIDING O-ATOM APPROACHING ALONG POSITIVE Z-AXIS

Distance to O Atom (bohr)[b]	SCF	SDQ-MBPT(4)
$^3B_1$ Ground State		
+2.5	-150.47027	-150.79727
+3.0	-150.69253	-151.02192
+4.0	-150.82630	-151.15808
+6.0	-150.85192	-151.17593
+8.0	-150.85212	-151.17578
$^3B_2$ First Excited State		
+2.5	-150.43655	-150.79260
+3.0	-150.67233	-151.02165
+3.5	-150.77522	-151.11363
+4.0	-150.82018	-151.15090
+4.5	-150.83914	-151.16630
+6.0	-150.85111	-151.17532
+8.0	-150.85196	-151.17562
$^3A_2$ Second Excited State		
+2.5	-150.20481	-150.58459
+3.0	-150.56853	-150.91886
+4.0	-150.80486	-151.13336
+6.0	-150.85295	-151.17704
+8.0	-150.85282	-151.17640

[a] Coordinates of H_2O molecule in bohrs are(O:0.0,0.0,-0.12371; H:0.0,±143085, 0.98161). Total energies in Hartrees.

[b] Distance is measured from center-of-mass of the H_2O molecule.

TABLE 4 . H₂0 AT EQUILIBRIUM.[a] COLLIDING O-ATOM APPROACHING
ALONG Y-AXIS

Distance to O-Atom(bohr)[b]	SCF	SDQ-MBPT(4)
	A' Ground State	
+2.5	-150.38065	-150.75549
+3.0	-150.65074	-151.00760
+3.5	·150.76810	-151.10805
+4.0	-150.82002	-151.15058
+5.0	-150.85025	-151.17531
+6.0	-150.85376	-151.17801
+8.0	-150.85215	-151.17829
	A" First Excited State	
+2.5	-150.33535	-150.70048
+3.0	-150.63058	-150.98266
+3.5	-150.75750	-151.09635
+4.0	-150.81343	-151.14387
+4.5	-150.83676	-151.16344
+5.0	-150.84609	-151.17116
+6.0	-150.85112	-151.17538
+8.0	-150.85209	-151.17825

[a] Coordinates of H₂0 molecule in bohrs are (O:0.0,0.0,-0.12371;
H:0.0,+1.43085,0.98168). Total energies in Hartrees.

[b] Distance is measured from the center-of-mass of the H₂0 molecule.

26

TABLE 5. H_2O AT EQUILIBRIUM.[a] COLLIDING O-ATOM
APPROACHING ALONG THE X-AXIS

Distance to O-atom (bohr)[b]	SCF	SDQ-MBPT(4)
A' Ground State (Approach in direction 0°)		
3.0	-150.72692	-151.07130
4.0	-150.83585	-151.16543
8.0	-150.85237	-151.17565
A' Ground State (Approach in direction +45°)		
3.0	-150.70467	-
4.0	-150.82954	-151.15960
6.0	-150.85286	-151.17663
A' Ground State (Approach in direction -45°)		
3.0	-150.71522	-151.05884
4.0	-150.83500	-151.16349
6.0	-150.85003	-151.17373

[a] Coordinates of H_2O molecule in bohrs are (0:0.0,0.0,-0.12371; H:0.0,+1.43085, 0.98164). Total energies in Hartrees.

[b] Distance is measured from the center-of-mass of the H_2O molecules.

TABLE 6. H_2O IN A LINEAR CONFIGURATION.[a]
COLLIDING O-ATOM APPROACHING ALONG THE Z-AXIS

Distance to O-atom (bohr)[b]	SCF	SDQ-MBPT(4)
$^3B_1$ Ground State		
-2.5	-150.5223	-150.8949
-3.0	-150.6876	-151.0306
-4.0	-510.7869	-151.1127
-6.0	-150.8017	-151.1216
$^3B_2$ First Excited State		
-2.5	-150.4982	-150.8603
-3.0	-150.6720	-150.0123
-4.0	-150.7826	-151.1079
-6.0	-150.8011	-151.1211
$^3A_2$ Second Excited State		
-2.5	-150.3062	-150.6480
-3.0	-150.5444	-
-4.0	-150.7556	-151.0779
-6.0	-150.7991	-151.1188

[a] Coordinates of H_2O in bohrs are (O : 0.0,0.0,0,0; H:0.0, $\pm$1.735236, 0.0). Total energies in Hartree atomic units.

[b] Distance is measured from the O-atom in the linear H_2O configuration.

TABLE 7. H_2O IN ASYMMETRIC STRETCH.[a] COLLIDING
O-ATOM APPROACHING ALONG THE Y-AXIS

Distance to O-Atom (bohr)[b]	SCF	SDQ-MBPT(4)
	A' Ground State	
+4.0	-150.81538	-151.14604
+3.5	-150.76315	-151.10243
+3.0	-150.64065	-150.99692
+2.5	-150.35848	-150.73519
-2.5	-150.37837	-150.75.94
-3.0	-150.64653	-151.00527
-3.5	-150.76036	-151.10242
-4.0	-150.81242	-151.14442
-6.0	-150.84798	-151.17208
-8.0	-150.84703	-151.17050

[a] Coordinates of H_2O molecule in bohrs are (O: 0.0,0.0,-0.12371, H1: 0.0,1.3640, 0.90480, H2: 0.0, -1.52390, 1.02520). Total energies in Hartrees atomic units.

[b] Distance is measured from the center-of-mass of the H_2O molecule at its original equilibrium position.

TABLE 8 . H_2O IN A BENT CONFIGURATION.[a] COLLIDING
O-ATOM IS APPROACHING ALONG THE Z-AXIS

Distance to O-Atom(bohr)[b]	SCF	SDQ-MBPT(4)
	$^3B_1$ Ground State	
-2.5	-150.57023	-150.95284
-3.0	-150.72326	-151.06877
-3.5	-150.80442	-151.13847
+2.5	-150.48542	-150.85942
+3.0	-150.70036	-
+3.5	-150.78971	-151.12909

[a] Coordinates of H_2O molecule in bohrs are (O:0.0,0.0,-0.10968; H1:0.0±1.52650, 0.87032). Total energies in Hartrees atomic units.

[b] Distance to the O-atom is measured from the center-of-mass of H_2O in its original equilibrium configuration.

TABLE 9. H2O AT EQUILIBRIUM.[a] COLLIDING O-ATOM APPROACHING IN THE PLANE OF MOLECULE. ENERGY AS A FUNCTION OF ANGLE, Θ. FROM THE Y-AXIS. A'GROUND STATE.

Distance to O-Atom[a] (bohrs)	30°		45°		60°		135°	
	SCF	SDQ-MBPT(4)	SCF	SDQ-MBPT(4)	SCF	SDQ-MBPT(4)	SCF	SDQ-MBPT(4)
3.0	-150.63198	-150.98841	-150.49173	-150.83692	-150.42928	-150.77233	-150.72047	-151.06531
3.5	-150.75915	-151.10918	-150.72783	-151.07303	-150.71267	-151.06272	-150.80468	-151.13770
4.0	-150.81239	-151.14788	-150.79857	-151.13699	-150.79337	-151.13099	-150.83705	-151.16486
4.5	-150.83666	-151.16488			-150.83118	-151.15822		
5.0					-150.84709	-151.17242		

31

Since the ground state surface is largely repulsive the number of geometries sampled in these calculations is not as large as would be necessary for a surface with local extrema.

In Figure 3 are shown the three surfaces obtained at the SCF (i.e., UHF) level. The strong repulsive character is evident. Also, there is only a modest difference in the $^3B_1$ and $^3B_2$ curves, with slightly more distinction from the $^3A_2$ curve. As shown in Figure 4, the behavior is unchanged at the SDQ-MBPT(4) level. In the case of the correlated treatment, the total energy is found to be much lower and the curves are displaced accordingly, but from the viewpoint of collision dynamics, cross sections will be affected only by the shape of the curves. A closer comparison demonstrates that the SCF and SDQ-MBPT(4) curves for H_2O at equilibrium are almost superimposable.

This behavior is further emphasized in Figure 5 when the SDQ-MBPT(4) and SCF curves are compared for an approach along the y-axis of the H_2O molecule. Although the difference between the correlated and uncorrelated curves is not constant for this approach, it is close to being so. The correlation energy is actually more nearly constant for collisions approaching along the z-axis.

In Figure 6 comparisons of the $^3B_2$ state at four different levels of approximation are presented. In addition to the similarity in shape of the SCF and SDQ-MBPT(4) curves, it is also evident that a restriction of the basis set to DZ (double-zeta) instead of the polarized DZP basis also has essentially no effect on the shape. A superposition of these curves would show no significant differences.
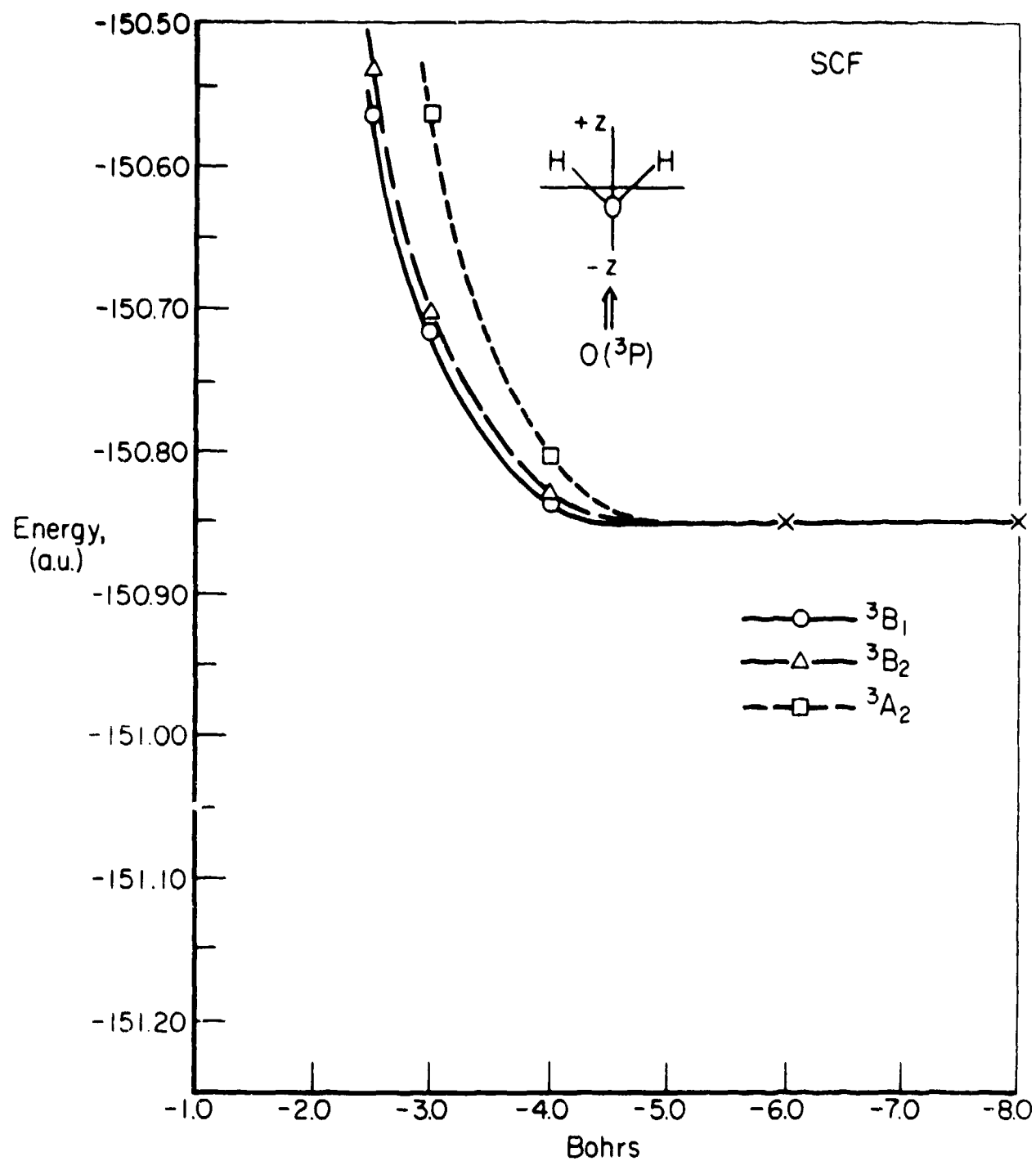
FIGURE 3. THE THREE ELECTRONIC STATES OBTAINED AT THE SCF
LEVEL FOR O(^{3}P) COLLIDING WITH H_2O AT EQUILIBRIUM
APPROACHING ALONG THE NEGATIVE Z-AXIS
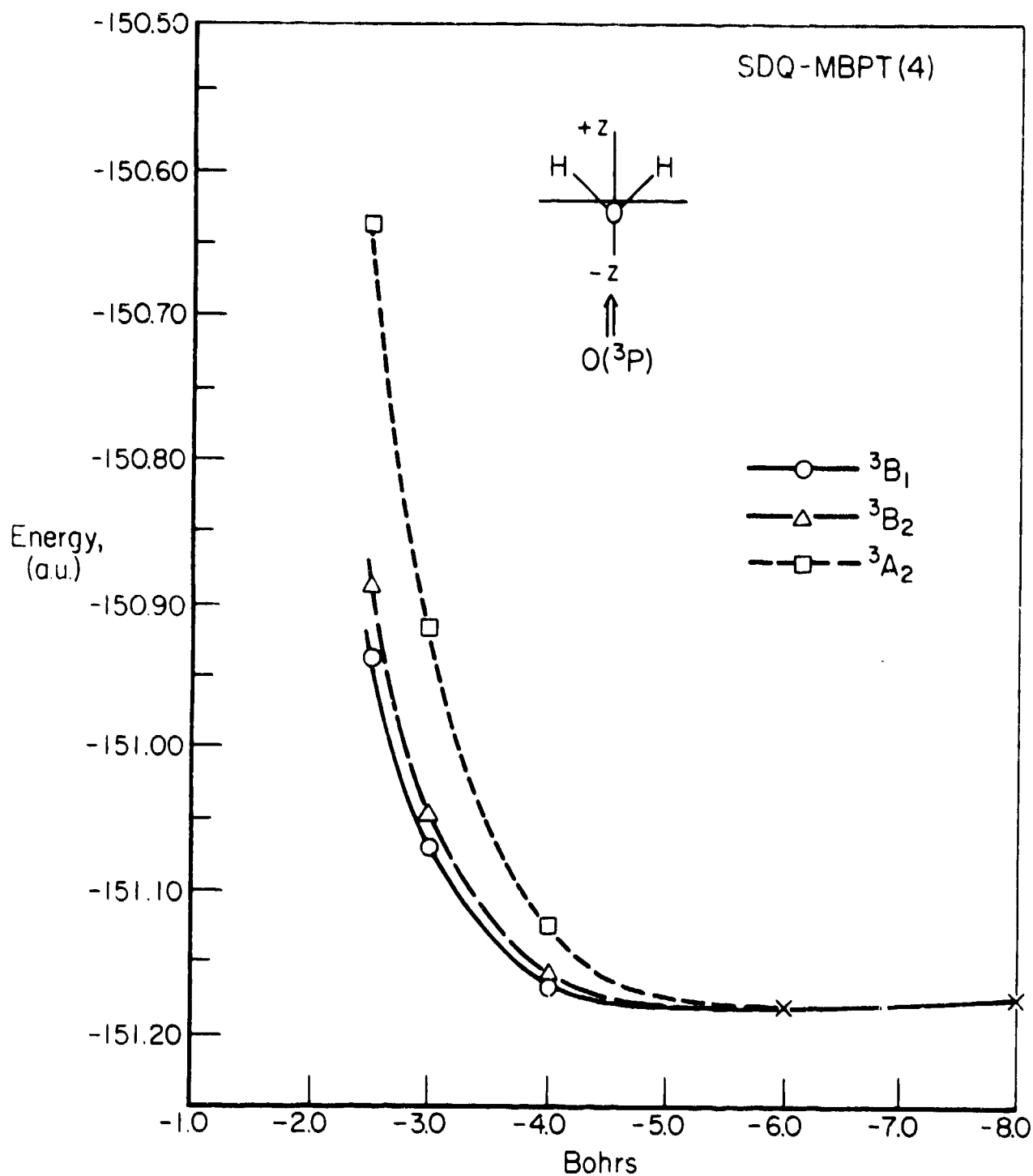
FIGURE 4. THE THREE ELECTRONIC STATES OBTAINED AT THE SDQ-MBPT(4) LEVEL FOR O(^{3}P) COLLIDING WITH H_2O AT EQUILIBRIUM, APPROACHING ALONG THE NEGATIVE Z-AXIS

FIGURE 5. A COMPARISON OF THE SCF AND SDQ-MBPT(4) CURVES FOR O(^{3}P) COLLIDING WITH H_2O AT EQUILIBRIUM, APPROACHING ALONG THE Y-AXIS.
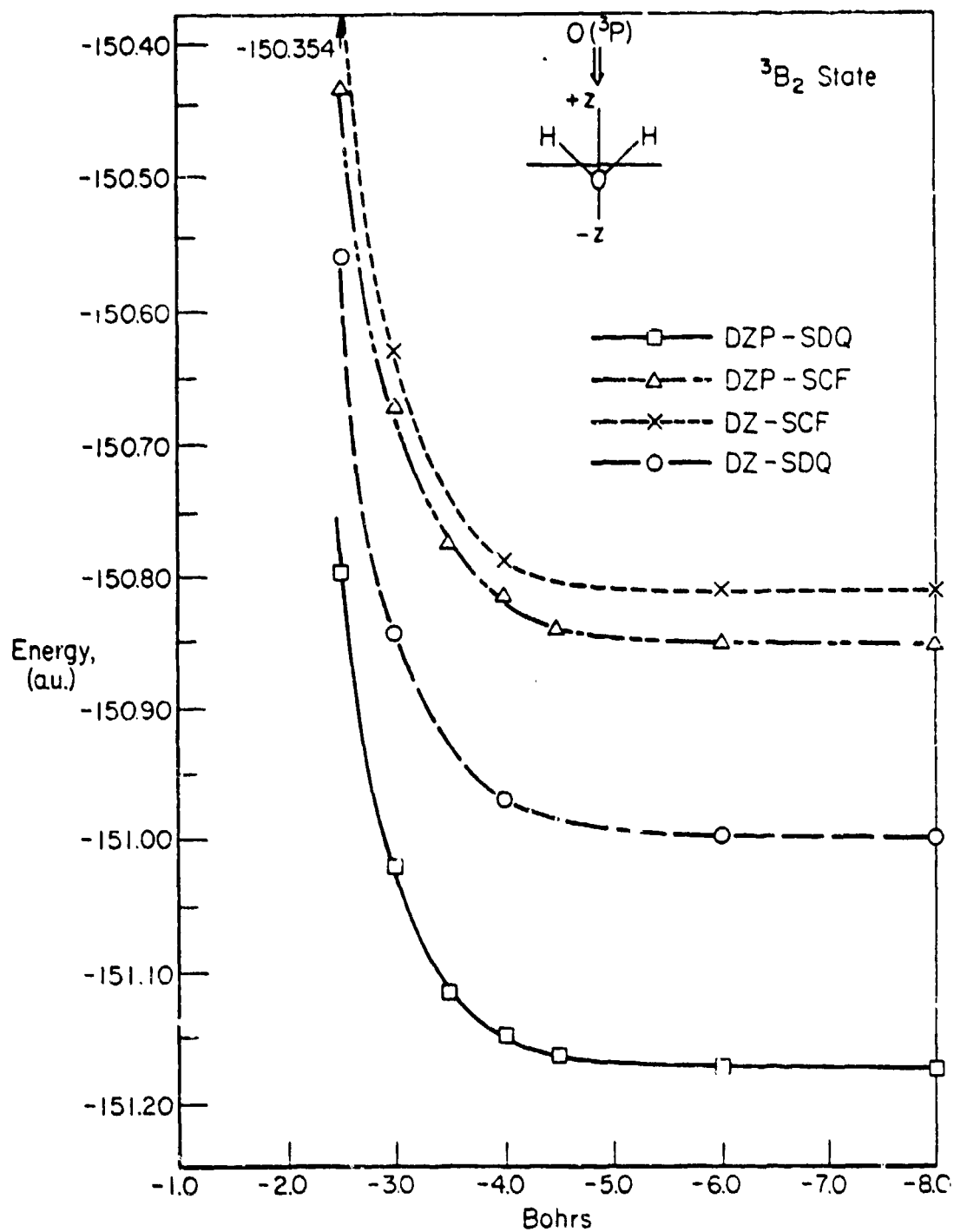
FIGURE 6. FOUR DIFFERENT APPROXIMATIONS TO THE $^3B_2$ STATE FOR $O(^3P)$ COLLIDING WITH H_2O AT EQUILIBRIUM APPROACHING ALONG THE POSITIVE Z-AXIS. DIFFERENT BASIS SETS, DOUBLE-ZETA(DZ) AND DOUBLE-ZETA PLUS POLARIZATION (DZP), AT BOTH THE SCF AND SDQ-MBPT(4) LEVEL ARE ILLUSTRATED.

This observation suggests two important points. The theoretical calculations at several different degrees of sophistication show very little differences, so that convergence to the correct potential surface has been effectively achieved. Further additions to the basis set or to the correlation effects included would not appear to cause important changes in the surface. Also, additional work at the much less expensive double-zeta level should therefore provide useful results. This is an important observation that permits using a DZ basis for the more expensive $O(^3P) + CO_2(^1\Sigma_g^+)$ PES.

Another benefit of the observed repulsive nature of the $O(^3P) + H_2O$ surface is that the analytical representation of the surface is much simpler than when minima must be reproduced.

Figures 7 and 8 illustrate the shape of the surface for two possible displacements of the H_2O molecule from equilibrium, the linear configuration and an asymmetric stretch. Again the overall shapes of the curves are similar, but there are observable differences caused by the displacement of H_2O as a function of O-atom position which must be realistically described in order for the dynamical calculations to result in reliable cross sections.

Probably the distorted structures having the most significant effect on the 001 cross sections involve asymmetric stretch displacements. This is also expected to be the route taken for the reaction $O(^3P) + H_2O(^1A_1) \rightarrow 2OH(^2\Pi)$, as shown in Figure 1. Since the bond energy of H - OH is 119 kcal/mole and O-H is 102.4, this reaction is endoergic by only 17 kcal/mole. At the collision velocities of interest in the current

37
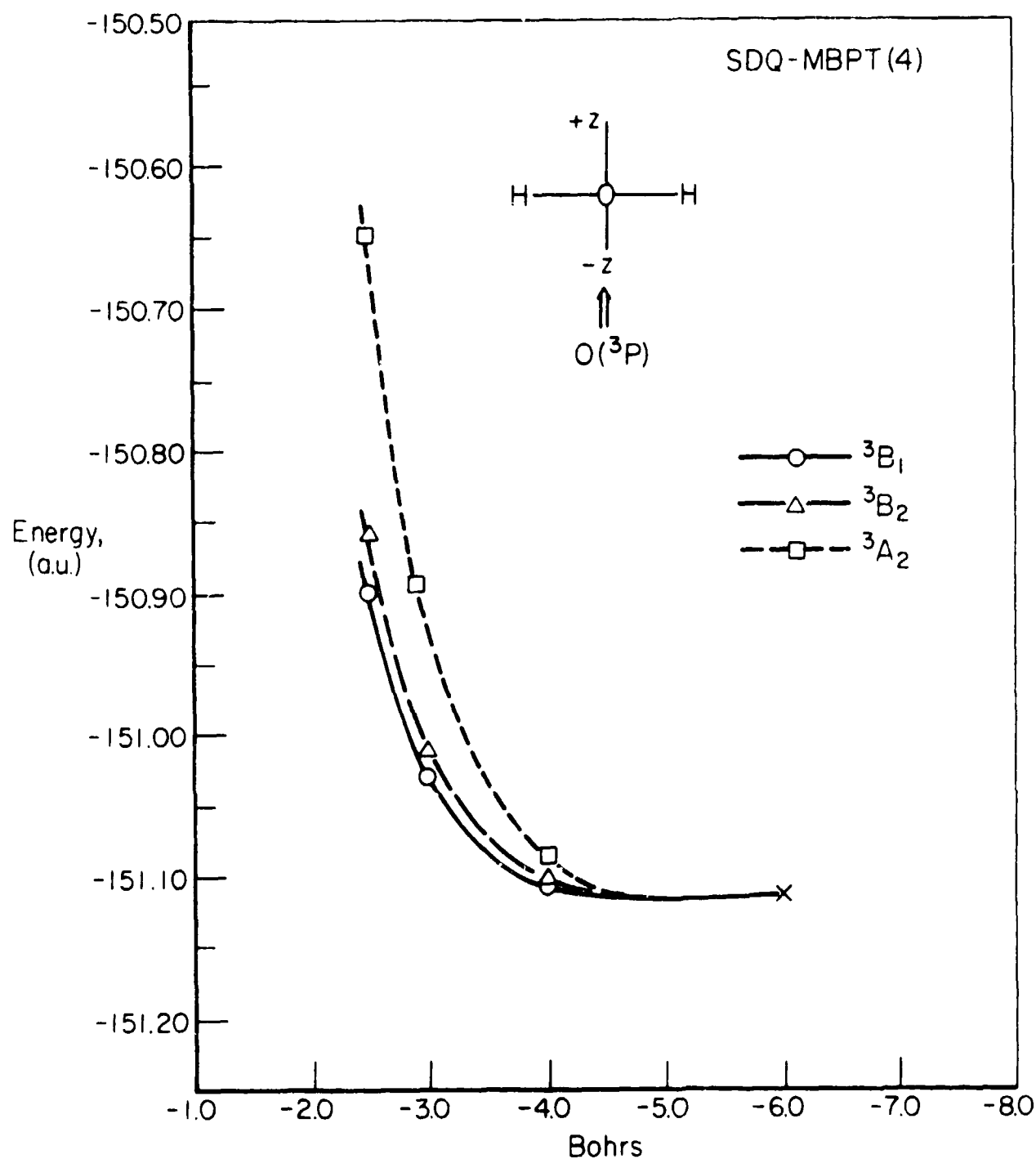
FIGURE 7.   ILLUSTRATION OF THE $^3B_1$, $^3B_2$, AND $^3A_2$ STATES WHEN
            H_2O ASSUMES A LINEAR CONFIGURATION. A COMPARISON
            OF FIGURE 7 WITH FIGURE 4 SHOWS THE EFFECT OF THE
            DISPLACEMENT
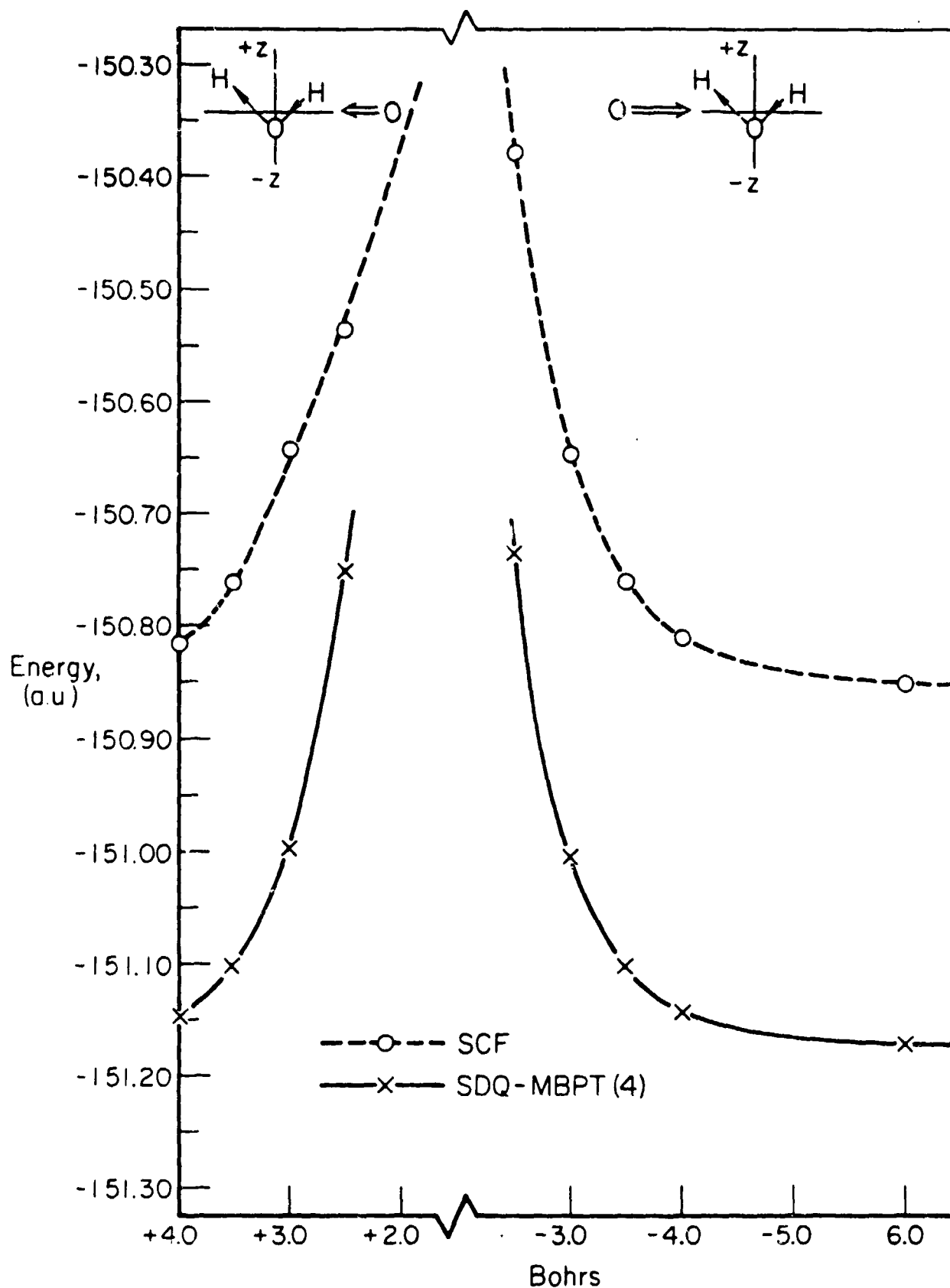
FIGURE 8.   ILLUSTRATION OF THE CURVES OBTAINED BY THE APPROACH OF AN O(^{3}P) ATOM ALONG THE POSITIVE AND NEGATIVE Y-AXIS WHEN H_2O IS DISPLACED IN AN ASYMMETRIC VIBRATION. NOTE THE ASYMMETRY OF THE REPULSIVE WALL FOR THE DIFFERENT APPROACHES

39

work, it does not appear likely that the reaction itself will withdraw much flux from the vibrational excitation channels, since little time is available to sample the reactive channel. However, for those trajectories in which large displacements of the OH bond occur, the potential surface used in this work may not be entirely accurate. Even though a number of points involving asymmetric stretches of H_2O have been computed, it is outside the scope of the present work to consider reactive collisions. Hence, there are not enough points computed to locate and classify a possible transition state region. This should be done in future work.

B. The Analytical Representation of the
$O(^3P) + H_2O$ Potential Energy Surface

The accurate representation of multidimensional potential energy surfaces has always been a formidable problem. A common approach is to employ an expression that incorporates as much physical insight as possible in the functional form, and which has a number of parameters that are adjusted to empirical data. Examples of this approach are found in applications of the London-Eyring-Polyani-Sato (LEPS), valence-bond (VB), diatomics-in-molecules (DIM), and many-body expansion methods for polyatomic systems.[15-18]

Recent developments in ab initio methods for calculating potential energy surfaces will require new, systematic approaches for obtaining useful analytical representations. Progress has been made in this area using, for example, multidimensional splines[19,20], polynominal root interpolation,[21] and many-body expansions.[22,23] An important goal is to develop methods that can be systematically applied and that require a relatively small number of ab initio points

The method used in the present work is based on the Sorbie-Murrell many-body representation of a potential energy surface,[24] which has been applied by Murrell and coworkers to a number of systems.[18] For studying non-reactive collisional excitation processes involving an oxygen atom colliding with a water molecule, the many-body expansion can be written

$$V(O, H_2O) = V_{OO}(R_{AB}) + V_{OH}(R_{AC}) + V_{OH}(R_{AD})$$

$$+ V_{H_2O}(R_{BC}, R_{BD}, R_{CD}) + V_{OHH}(R_{AC}, R_{AD}, R_{CD})$$

41

$$+ V_{OOH}(R_{AB}, R_{BC}, R_{AC}) + V_{OOH}(R_{AB}, R_{BD}, R_{AD})$$

$$+ V_{OOHH}(R_{AB}, R_{AC}, R_{AD}, R_{BC}, R_{BD}, R_{CD}).$$

In this expression A and B represent the reagent atom and oxygen atom in the molecule, respectively, while C and D represent the hydrogen atoms.

Since reactive channels are excluded from the present study, one can choose the fragment potentials to ensure that the contribution of the four-body term is small. Since the ab initio points show a repulsive surface (in the region sampled), the two-body terms are chosen to be exponentials. The term V_{H_2O} is taken to be an accurate ground-state surface for the water molecule.[8,25] All of the remaining three- and four-body terms are represented as products of polynominals times suitable cutoff functions.

The choice of exponentials for the intermolecular pair potentials is made so that the simple sum-of-pairs plus intramolecular force field representation

$$V^{(2)}(0, H_2O) = V_{OO}(R_{AB}) + V_{OH}(R_{AC}) + V_{OH}(R_{AD}) + V_{H_2O}(R_{BC}, R_{BD}, R_{CD})$$

contains the essential features of the surface. The two-body terms are represented as sums of two exponential functions

$$V_{AB}(R) = A_1 e^{-\alpha_1 R} + A_2 e^{-\alpha_2 R} - C/R^6$$

with the exponents adjusted to the slope of the surface along two cuts. The linear coefficients are determined by linear regression using a large number of points for which H_2O is at its equilibrium. The resulting

42

fit is then corrected by adding in the additional three-body and then four-body terms, using linear regression at each stage to determine the polynomial coefficients. This time, points that represent vibrational displacements of H_2O away from equilibrium are included. This allows the fit to properly describe the variation of the force constants of the water molecule with the approach of the oxygen atom. It should be mentioned that sequential inclusion of the higher order terms is necessary to avoid unphysical behavior of the fit in regions where ab initio points are not available. This undesirable behavior always occurs if all of the coefficients are adjusted simultaneously.

The decay functions used to damp out the polynomials are of the form[11]

$$\prod_{i=1}^{N} [1 - \tanh (\gamma_i S_i/2)] ,$$

where N is 3 or 6, and $S_i = R_i - R_{io}$. Both R_{io} and γ_i are chosen to shape the functions so that the ab initio points could be fit without the polynomial coefficients becoming too large. This helps in smoothing the overall representation of the surface.

A very important feature of the many-body approach is the convenience with which information about the fragments can be included. Since this study emphasizes collisional energy transfer, it is important to have a reliable surface for the water molecule that reproduces the known force constants.

The first potential used was a very accurate quartic force field obtained by SDQ-MBPT(4).[8] Because high velocity collisions are found to greatly perturb the bending mode, a potential that is

43

reliable further from equilibrium is required. Consequently, the Sorbie-Murrell representation of the water molecule is adopted, but with parameters determined so that the fit reproduced the MBPT quartic force field[25] rather than experiment.[24]

In Table 10 a comparison is made of the force constants obtained in Reference 8 with those of the fit,[25] and the agreement is seen to be excellent. As seen in Figure 9, however, the bending potential from the fit for H_2O is much more realistic away from equilibrium than is the quartic force field. This is demonstrated by the existence of a saddle point for the bending motion for a linear geometry of H_2O for the many-body fit with a barrier of 1.296 eV above the water equilibrium energy, while the quartic force field does not even have a saddle point. Experimental estimates are that the barrier is 1.37 eV above the equilibrium energy,[19] while calculations using the present DZP basis give 1.5 eV. Using the many-body fit for V_{H_2O} results in an order of magnitude increase in the asymmetric stretch excitation cross section at 1.5 eV relative energy. It would appear then that the choice of V_{H_2O} is critical for studies of collisional energy transfer in water. Contours for the stretching displacements of H_2O are in Figure 10.

The ab initio points are selected with the dynamics applications in mind. Since high-velocity collisional excitation of the vibrational modes is of interest, most of the calculations are made for $O(^3P)$ in the plane of the H_2O molecule. In Figure 2 the distribution of points in this plane is shown for H_2O at its equilibrium geometry. As discussed previously calculations are also made for out-of-plane geometries and for nonequilibrium H_2O configurations.

44

reliable further from equilibrium is required. Consequently, the Sorbie-Murrell representation of the water molecule is adopted, but with parameters determined so that the fit reproduced the MBPT quartic force field[25] rather than experiment.[24]

In Table 10 a comparison is made of the force constants obtained in Reference 8 with those of the fit,[25] and the agreement is seen to be excellent. As seen in Figure 9, however, the bending potential from the fit for H_2O is much more realistic away from equilibrium than is the quartic force field. This is demonstrated by the existence of a saddle point for the bending motion for a linear geometry of H_2O for the many-body fit with a barrier of 1.296 eV above the water equilibrium energy, while the quartic force field does not even have a saddle point. Experimental estimates are that the barrier is 1.37 eV above the equilibrium energy,[19] while calculations using the present DZP basis give 1.5 eV. Using the many-body fit for V_{H_2O} results in an order of magnitude increase in the asymmetric stretch excitation cross section at 1.5 eV relative energy. It would appear then that the choice of V_{H_2O} is critical for studies of collisional energy transfer in water. Contours for the stretching displacements of H_2O are in Figure 10.

The ab initio points are selected with the dynamics applications in mind. Since high-velocity collisional excitation of the vibrational modes is of interest, most of the calculations are made for $O(^3P)$ in the plane of the H_2O molecule. In Figure 2 the distribution of points in this plane is shown for H_2O at its equilibrium geometry. As discussed previously calculations are also made for out-of-plane geometries and for nonequilibrium H_2O configurations.

44

TABLE 10. FORCE CONSTANTS FOR H_2O

	EXP^a	$MBPT^b$	FIT^c
ω_1	3831.5	3865.0	3864.9
ω_2	1648.8	1687.4	1687.4
ω_3	3942.2	3975.0	3975.0
k_{111}	-302.5	-304.2	-304.2
k_{222}	63.6	42.9	42.9
k_{122}	167.4	148.6	148.6
k_{211}	-53.1	-61.8	-61.8
k_{133}	-927.8	-914.1	-914.1
k_{233}	-138.8	-111.7	-111.6
k_{1111}	31.9	31.5	31.5
k_{2222}	2.1	-2.6	-2.6
k_{3333}	35.4	32.0	32.0
k_{1122}	-85.6	-75.1	-74.8
k_{1133}	201.3	190.3	190.4
k_{2233}	-101.1	-91.7	-91.4

[+] Units are cm^{-1}.

[a] Hoy-Mills-Strey.

[b] MBPT

[c] Many-Body Fit.
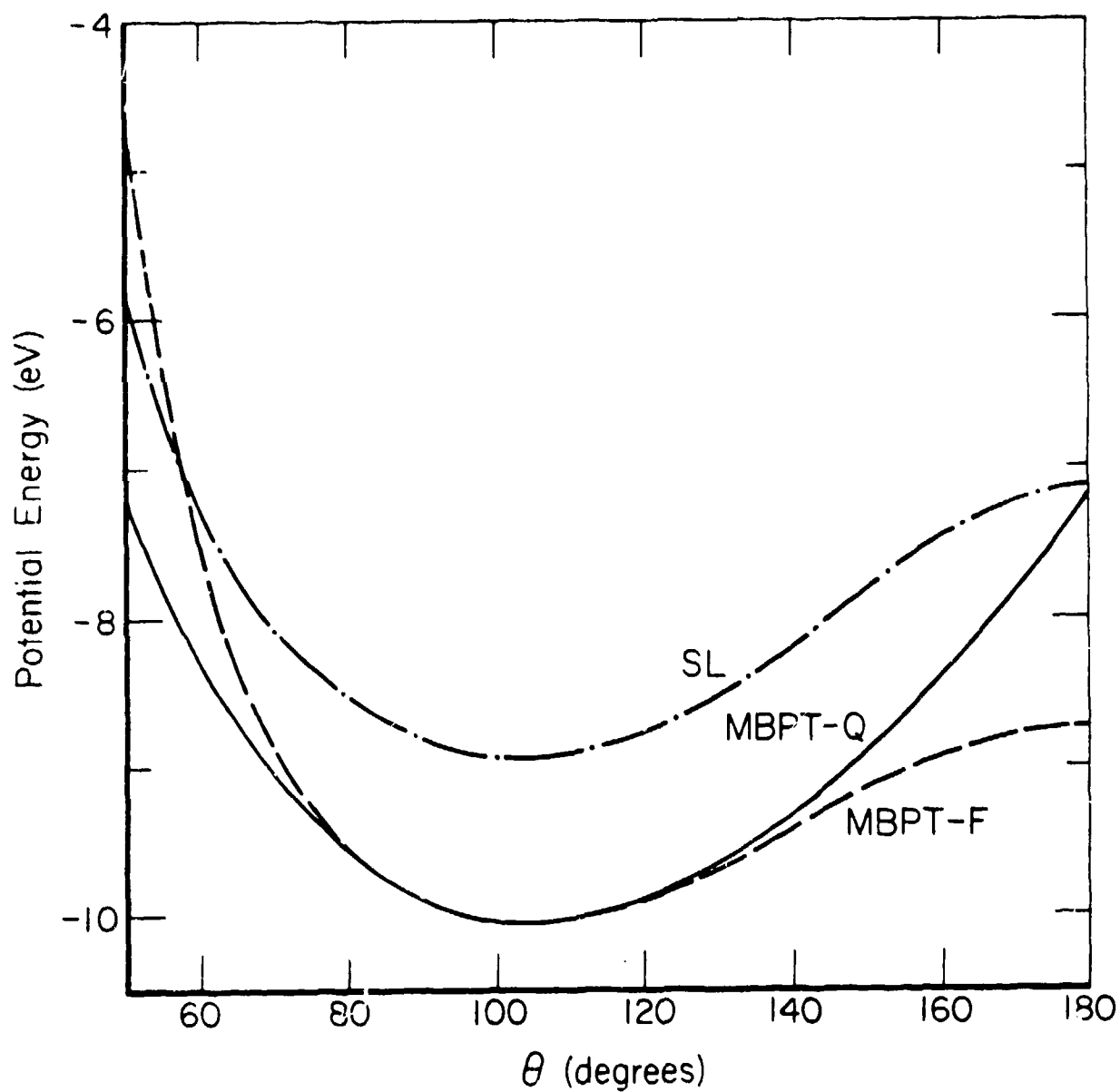
FIGURE 9. BENDING POTENTIAL FOR H_2O FOR OH AT THE MOLECULAR EQUILIBRIUM BOND LENGTH. THE CURVES MARKED MBPT-Q AND MBPT-F ARE THE QUARTIC AND MANY-BODY REPRESENTATIONS RESPECTIVELY. THE CURVE SL IS FROM THE MANY BODY FIT OF SCHINKE AND LESTER TO ANOTHER AB INITIO CALCULATION.

46
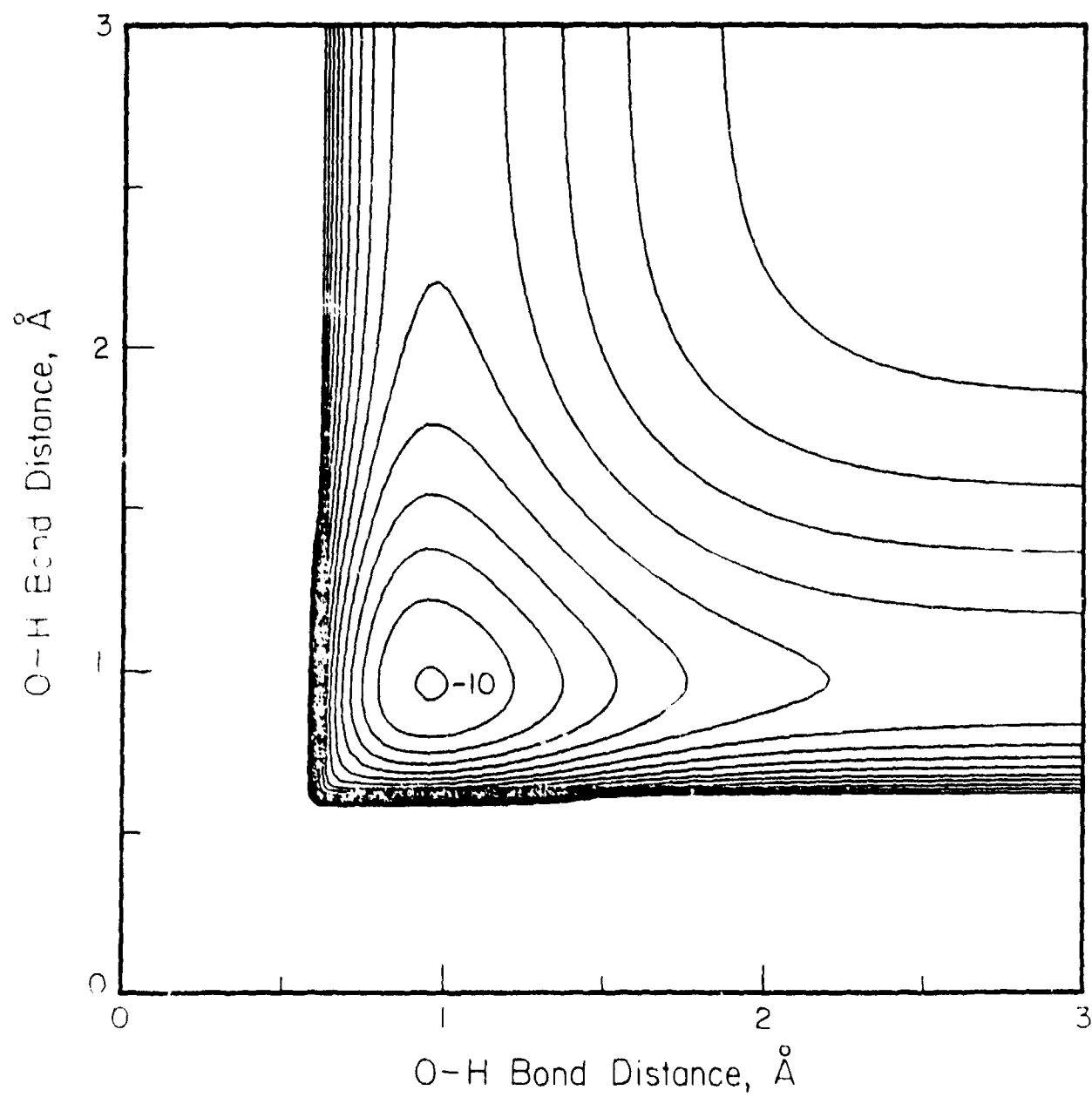
FIGURE 10. POTENTIAL CONTOURS FOR STRETCHING DISPLACEMENTS FOR H_2O. CONTOUR INCREMENT IS 1 eV

47

A number of fits to the computed ab initio points are made, using various combinations of points and terms in the many-body expansion. Those that are discussed here are used in trajectory calculations that will be presented in a later section. The various fits are denoted by combinations of alphanumeric characters, such as E_{2a}. This fit is determined using only two-body terms for the intermolecular potential. E_{3a} uses three-body terms to second order, and F_{4a} uses four-body terms to second order. $E_3^{(4)}$ uses three-body terms to fourth order. E_{3a}, F_{3b}, and F_{3d} differ essentially in the weights used for the linear regression, and the choice of parameters for the cutoff functions.

In Figure 11 are shown bending potentials for motion of the incoming O-atom in the plane of the H_2O molecule at a constant distance of 3.5 a_0 from the center-of-mass of H_2O. $0°$ corresponds in Figures 11-13 to an approach along the z-axis toward the two hydrogen atoms, and $180°$ corresponds to an approach toward the O-atom end of the molecule. The two curves labeled F represent the best fits, although the two-body fit E_{2a} is realistic. Subtle changes in the choice of weights or of the nonlinear parameters can significantly affect the quality of the fit. The three-body fits in Figure 11 involve only second-order polynomial terms.

The influence of higher-order terms is illustrated in Figure 12. Fit $E_3^{(4)}$ employs three-body terms to fourth order, and provides a fit to most of the 74 points used to within about 1%. Although this is an accurate fit to the computed points, the possibility of the occurrence of unphysical oscillations prevents its use in trajectory studies as many of the polynomial coefficients are quite large. Further work at this level would be likely to produce a useful surface.

48
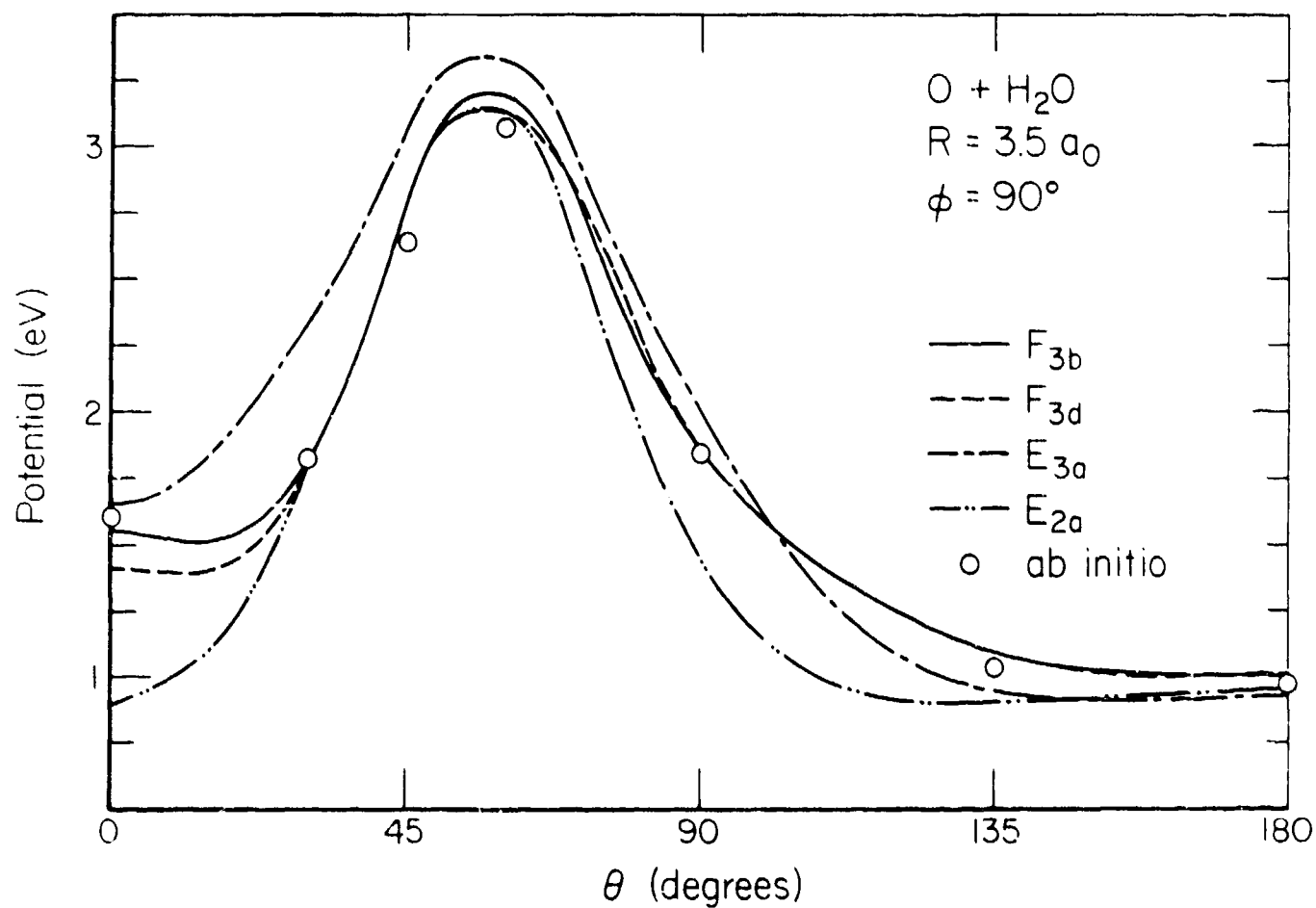
FIGURE II.   BENDING POTENTIAL FOR O(^{3}P) ABOUT H$_2$O IN THE PLANE OF THE MOLECULE AT A CONSTANT DISTANCE OF 3.5 a$_0$ FROM THE MOLECULAR CENTER-OF-MASS. THE VARIOUS FITS ARE DISCUSSED IN THE TEXT. COMPARISON IS BETWEEN A SUM-OF-PAIRS REPRESENTATION AND THESE THREE-BODY FITS TO SECOND ORDER

49
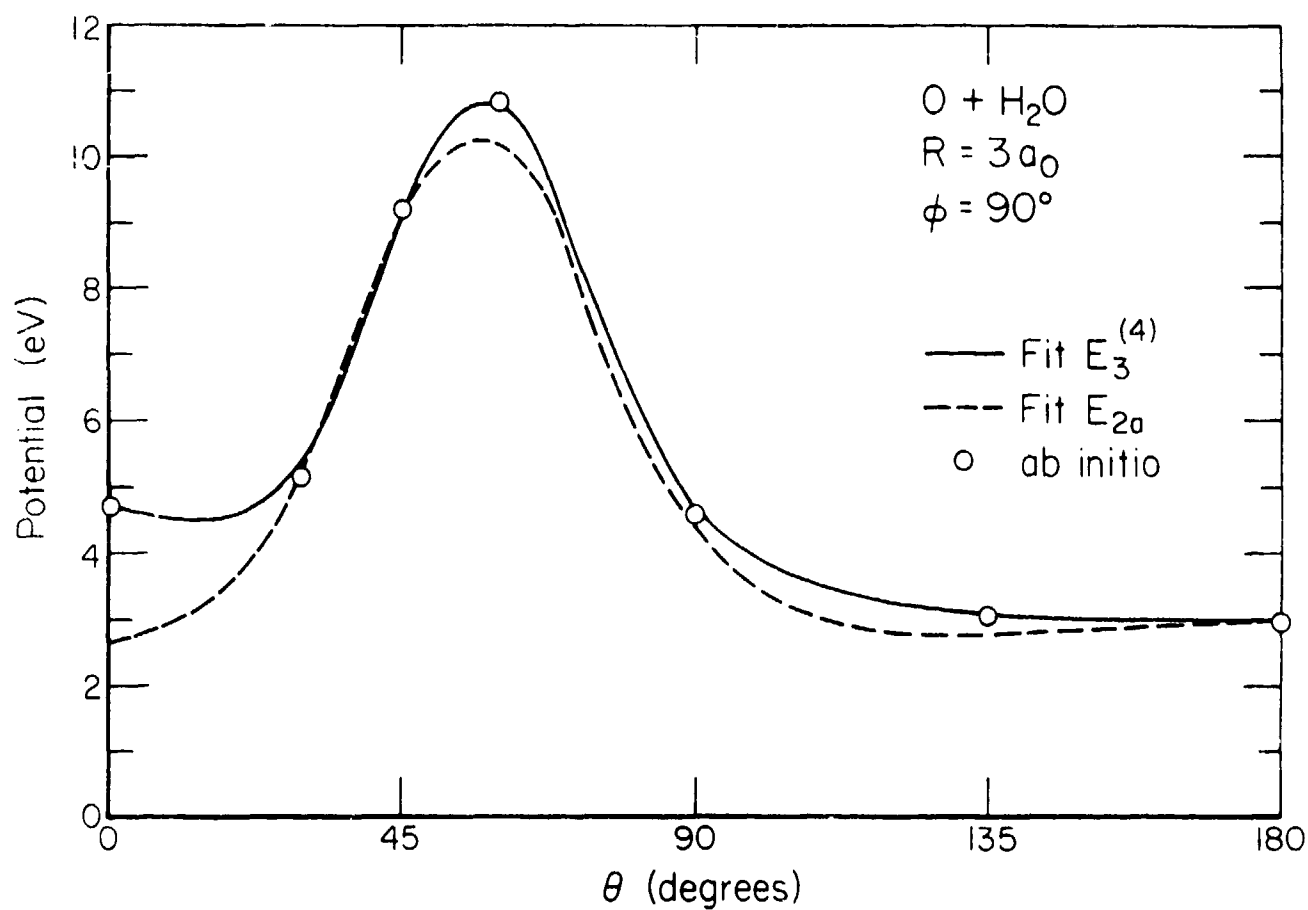
FIGURE 12. SIMILAR TO FIGURE 11, EXCEPT FOR A THREE-BODY FIT
TO FOURTH ORDER

In Figure 13 the influence of four-body terms (F_{4a}) is shown. In this fit, the three-body coefficients of fit F_{3d} are used, and only the four-body coefficients are adjusted by regression. It can be seen that the four-body contribution is negligible except between 0° and 30°, and there it is small. This is the case for all other cuts that were examined, and is the result of having obtained a good three-body fit.

In Figure 14, the incoming O-atom is fixed at various distances from the molecule center-of-mass, and the molecule is bent to a linear configuration. The four-body fit is shown, and a small barrier is seen to occur for the 3.0 a_0 curve. This is an artifact produced by not having a sufficient number of ab initio points. In Figure 15 the differences in the fits are presented for a symmetric stretch displacement. The three-body curves are similar in shape, but the four-body curve is somewhat softer, and not necessarily more accurate. The ab initio points are not shown on these two figures because the geometries used do not exactly correspond to the motion described in these figures. Figure 16 presents a yz plane view of the potential contours for the O + H_2O surface, with H_2O at equilibrium. The surface cut is seen to be fairly circular, only skewed somewhat due to the influence of the hydrogen atoms.

Studies of many cuts through the various surface fits demonstrate that a sufficiently accurate representation of the $O(^3P)$ + H_2O PES is obtained (considering the limited number of points available) using three-body terms through second order. Quasiclassical trajectories are used to examine differences in the collisional excitation cross-sections resulting from several surfaces. The results of this comparison will be given in the last section.

51
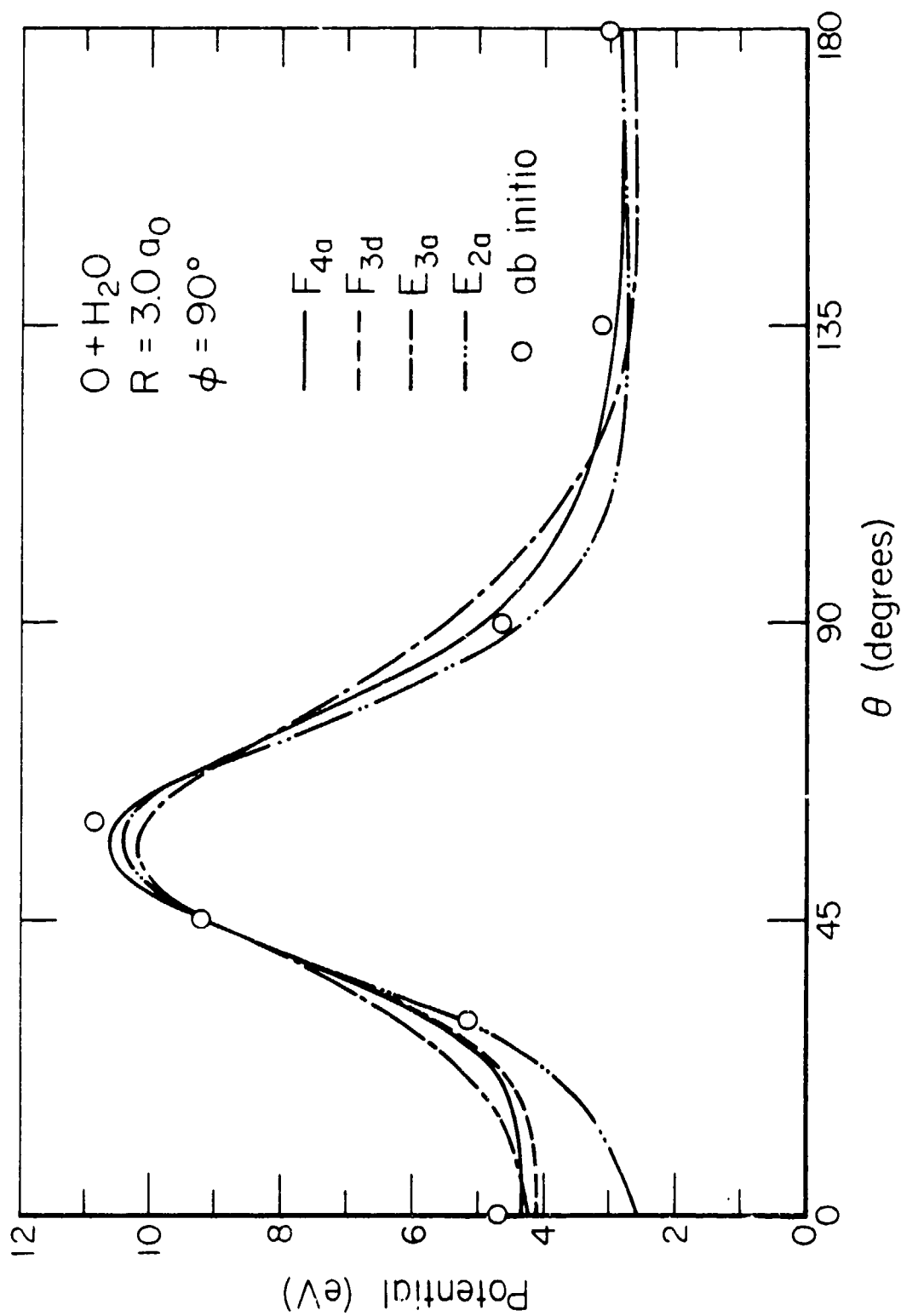
FIGURE 13. SIMILAR TO FIGURE 11, EXCEPT FOR THE INCLUSION OF A FOUR-BODY FIT TO SECOND ORDER, $F_4{}^a$. THE DISTANCE TO THE CENTER-OF-MASS OF THE MOLECULE IS FIXED HERE AT 3.0 a_0.
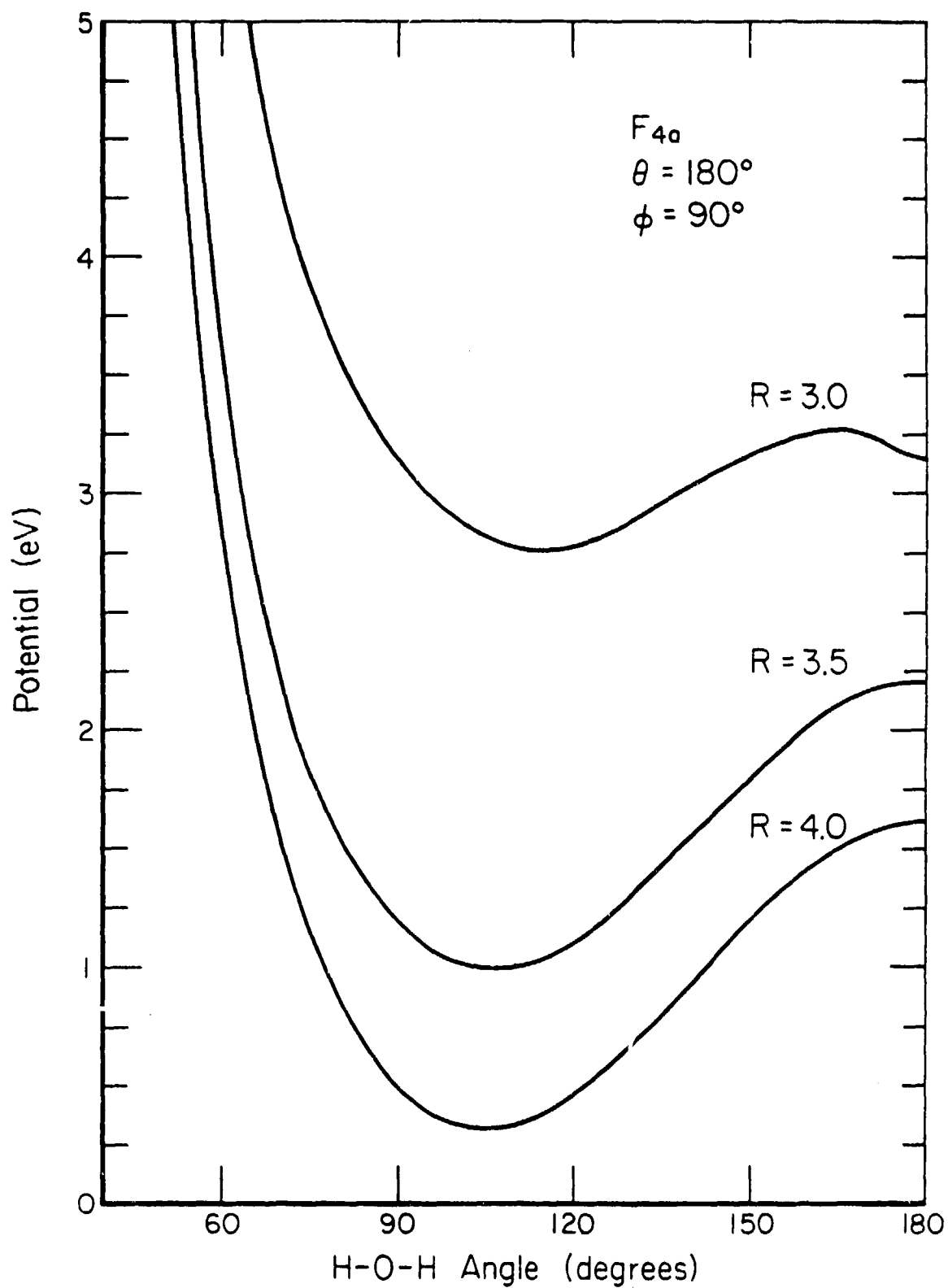
FIGURE 14. BENDING FOR THE WATER MOLECULAR AS A FUNCTION
OF THE APPROACH OF O(^{3}P) ALONG THE C_{2v} AXIS TOWARD
THE OXYGEN END OF THE MOLECULE. THE CURVES ARE
ALL FOR THE FOUR-BODY FIT.

53
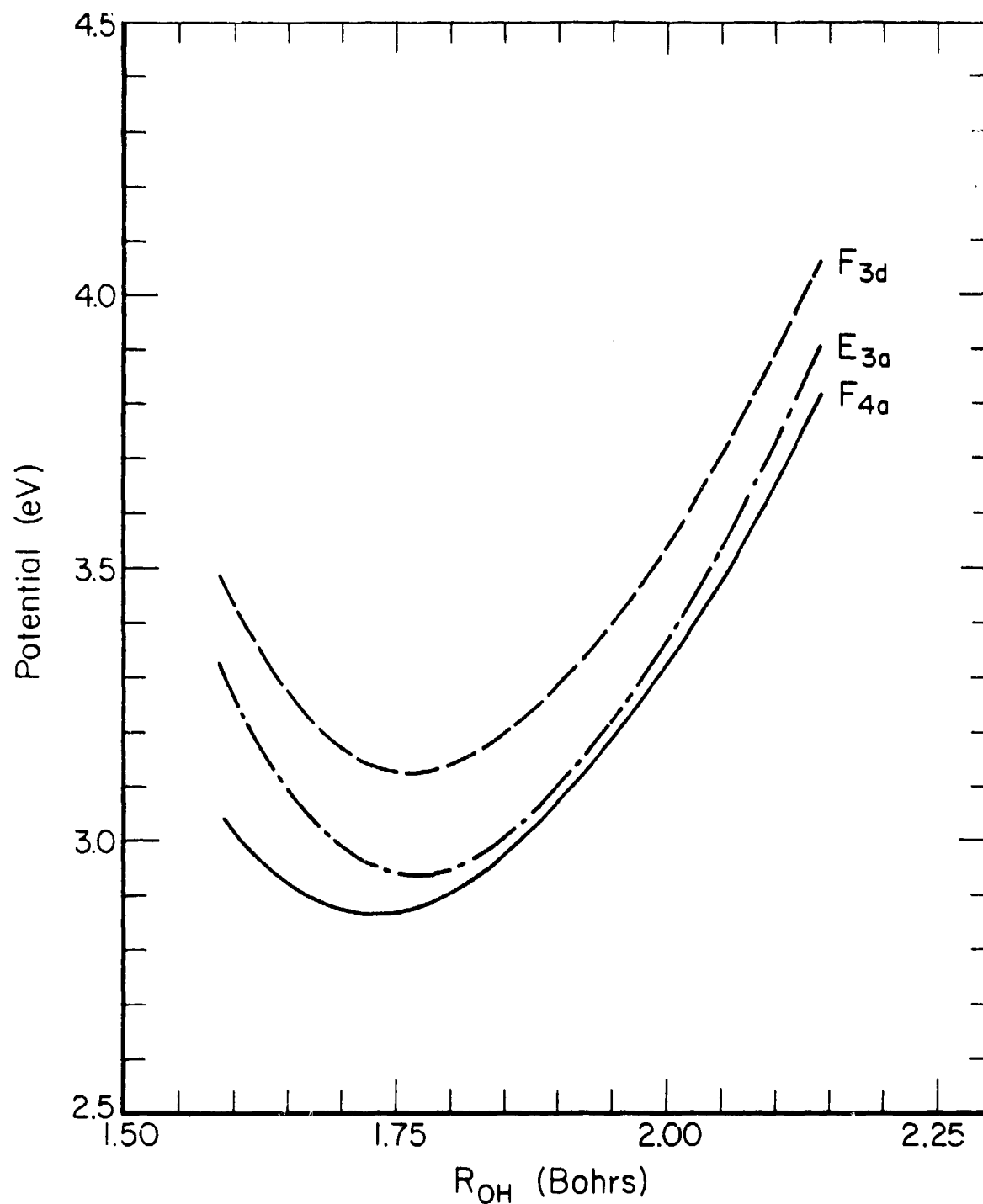
FIGURE 15. A COMPARISON OF THREE- AND FOUR-BODY FITS FOR A
SYMMETRIC STRETCH, WITH $O(^3P)$ 3.0 a_0 FROM THE
OXYGEN AND OF THE MOLECULE ALONG THE C_{2V} AXIS.
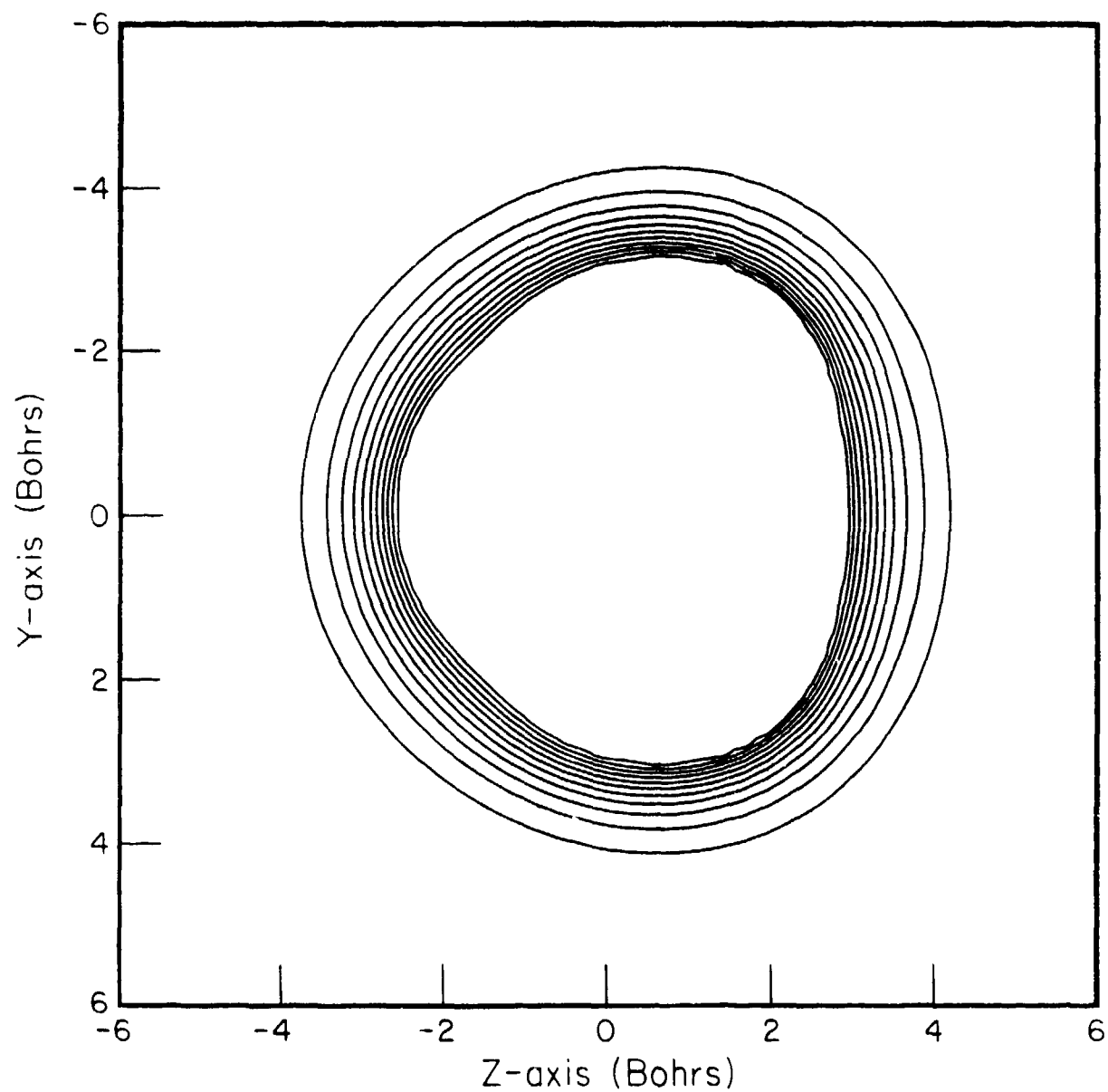
FIGURE 16.   POTENTIAL CONTOURS IN THE PLANE OF H_2O FOR $O + H_2O$.   THE H_2O MOLECULE IS FIXED AT EQUILIBRIUM.   CONTOUR INCREMENT IS 0.5 eV.

C. Some Aspects of the Quasiclassical Trajectory Method as Applied to Collisional Excitation of H_2O

Collisional excitation cross sections for $O + H_2O$ are determined using the quasiclassical trajectory method. Although the basic theory of trajectory calculations for atom-diatom collisions was developed long ago,[26] the generalization of this to collisions involving triatomics and higher polyatomics has been investigated in detail only recently. The trajectory integration itself is not too difficult (although it can involve significant computer time) but the specification of the initial and final conditions of the polyatomic collision partners requires the rather difficult determination of their semiclassical vibration-rotation eigenstates. If the molecular internal motion is quasiperiodic,[27] then the semiclassical eigenstates can be determined by finding the good action variables which describe vibration-rotation motion, and equating these actions to half integral multiples of $\hbar$. This is the procedure used for each trajectory in this study, both for the initial state preparation, and for the final state assignment.

The determination of the good actions describing vibration-rotation motion requires the solution of the molecular Hamilton-Jacobi equation which is a nonlinear partial differential equation in 3N-5 variables (including rotation). Even for N = 3 (a triatomic molecule) an exact solution to this equation is computationally extremely complex and is not practical for collisional applications. Several approximations can be used to simplify this treatment, however, including: (1) the separation

56

of vibration from rotation (valid in the limit of an adequate vibration-
rotation time scale separation); and (2) the use of classical perturba-
tion theory (in 2nd and 3rd order) to solve the three dimensional
Hamilton-Jacobi equation for vibration which remains after the separation
from rotation. Details of both the separation procedures and the
perturbation theory solution are discussed elsewhere.[28,29] For the
present application, the validity of the first approximation is tested
by comparing the ensemble average change in translational energy with
the sum of the vibrational plus rotational energy changes. If energy
is conserved and if the Hamiltonian is exactly separable, then these two
energy changes should have the same magnitude but opposite signs. All of
our calculations indicate that this holds to better than 1%, even for
highly rotationally excited H_2O. The accuracy of the perturbation theory
method is tested by calculating the final good actions from a given
trajectory at several different end points. If the actions are truly
constants of the motion, they should be independent of end point. For
H_2O with zero rotational energy, the actions oscillate by $\pm 0.05\hbar$. This
is much larger than is obtained in the analogous treatment of heavier
molecules like CO_2,[28] but is consistent with expected errors due to
anharmonic effects in H_2O and is probably acceptable for calculating
histogram and moment probabilities. When the H_2O molecule has rotational
energy equal to or greater than the vibrational zero point energy, the
good actions oscillate very substantially with end point location (by as
much as $0.5\hbar$). Obviously such large oscillations could lead to inaccurate
histogram probabilities and moments. Fortunately, for the stretching

excitations, the amount of rotational excitation is much smaller than the zero point energy, so these unphysical oscillations in the final actions are closer to $0.05\hbar$ than to $0.5\hbar$.

One very effective approach for partitioning the molecular Hamiltonian to simplify vibration-rotation interaction effects involves the use of classical rotation sudden approximations.[30] These are primarily applicable to high-velocity collisions, and have been quite effectively applied to the $Li^+ + CO_2$ system.[31] In the present application, both sudden and fully coupled cross sections for vibrational excitation are obtained.

Using either the sudden or fully coupled methods, a major problem with the use of a trajectory method to calculate state-to-state cross sections concerns the assignment of a final state to each trajectory. One well studied approach is the classical histogram method. In this, the final good actions are rounded off to the nearest half integer multiple of $\hbar$, and the trajectories are then binned by the final states thus defined. This is known to work well when many states are populated in the excitation process. At the velocities of interest in this study, however, only the first excited symmetric or asymmetric stretch states are found to be excited. This makes the histogram treatment of these excitations somewhat uncertain. Moreover, the probability of stretch excitation is often small enough in this system (on the order of 0.001) that the accumulation of good statistics requires the integration of a very large number of trajectories (many thousands). A further problem with the histogram method is its inability to determine cross sections for transitions which are classically forbidden.[26]

An alternative procedure for determining cross sections (one which circumvents the above mentioned problems) involves the use of moments of the final action distribution to predict the final state distribution. In essence, this "moment method" seeks to construct the quantum distribution based on knowledge of a few classical moments. Justification for this procedure is based on the approximate equality of low order classical and quantum moments for some systems, and on the fact that it is possible to characterize quantum probability distributions completely in terms of one or two moments. Although moment methods have often been studied for atom-diatom systems,[26] with comparisons of exact quantum and moment method probabilities available, no analogous study of moment methods for polyatomic systems have been done. In addition, it is not particularly clear how best to generalize many of the existing moment methods to the treatment of polyatomic systems. The incorporation of correlations between different degrees of freedom in the final state distributions has not been considered, for example.

In view of the desirability of a moment approach, but also the uncertainty in the application of existing ones, a very simple method is adopted which uses moments to construct and extrapolate the classical action distribution, then applies the histogram method to the moment generated distribution to obtain cross sections. Assuming that the exact classical action distributions can be accurately represented in terms of just a small number of moments, this approach will generate moment transition probabilities which equal the histogram ones for classically allowed processes. This is itself quite useful, for it

provides a method for generating cross sections for low probability
allowed processes without integrating many trajectories. In addition,
it provides an extrapolation of the action distribution which can be
used to estimate weakly forbidden cross sections.

The motivation for using an extrapolation of this sort is
based on the actual appearance of the action distribution.
When summed over all actions except the one of interest, this distribution
always exhibits an exponential decrease with action on both sides of its
peak value. For any finite number of trajectories, the calculated
distribution will, of course, truncate when the distribution decays
to a low enough probability. The moment method smoothly extrapolates
the truncated result to enable calculations of low probability allowed
and forbidden events. For allowed processes, the method has obvious
justification while for forbidden processes, it gives a smooth extra-
polation of the allowed results. This extrapolation is probably inaccurate
for all but weakly forbidden processes, but since the transitions of
interest in this work are always either allowed or weakly forbidden at the
velocities of interest, the extrapolation is small and presumably accurate.
For most of the moment results to be presented, a simple exponential
function $\exp(-\gamma|N-\bar{N}|)$ is found to describe the action distribution
adequately. (Here N is the action, $\bar{N}$ the average of N and γ is a decay
parameter which can be related to the second moment of N). Histogram
probabilities are easily determined using this distribution for each
mode, and the total (three mode) distribution is obtained by taking
products of the individual mode distributions.

In this study, a variable-step fixed order Adams-Moulton method is used to integrate the equations of motion. Maximum separation is fixed at 10 a_0, and a suitable maximum value for the impact parameter is found to be 4.2 a_0. The initial step-size is fixed at five atomic seconds. Sampling of impact parameters is done by randomizing the orbital angular momentum. The range of collision energies studied is 0.5 eV to 2.5 eV, and usually 500 trajectories are run for each initial translational energy and rotational state. Initial rotational energies are investigated up to a value corresponding to about J=20.

D. Cross-Sections for Collisional Excitation
of H_2O by $O(^3P)$ Atom Impact

Quasiclassical trajectory calculations are performed on a
number of different fits to the _ab initio_ $O(^3P)$ + H_2O ground state
potential energy surface, using full three-dimensional calculations and
a classical rotational sudden approximation. The use of several fits
allows the effect of variations in the potential surface on the
computed cross sections to be investigated. In all cases the water
molecule is in its ground vibrational state.

In Table 11 moment cross sections are compared for several
different fits, all involving two-body terms to second order. This particular
translational and rotational energy are chosen because results are
available for all three surfaces. Considering the variations in the
fits, the cross-sections are in reasonable agreement, the largest
percent error being for the asymmetric stretch between fits E_{3a} and
F_{3b}, but still less than a factor of two. Trajectories are not run
for the sum-of-pairs representation for the rotational energy in
Table 11, but at E_{ROT} = .16 the 001 cross section on that surface is
within 50% of the cross section on surface E_{3a}. This comparison suggests
that errors in the results due to inaccuracies in the fit to the computed
points are probably less than a factor of two.

The comparison between moment cross sections and histogram
cross sections in Table 12 shows that the agreement is usually
excellent for large amounts of rotational excitation. For collision
energies above 1eV, the agreement is usually better than a factor of two.

TABLE 11.   COMPARISON OF MOMENT CROSS-SECTIONS*
            FOR SEVERAL SURFACE FITS

Fit	(100)	(010)	(001)
E_{3a}	0.31	0.99	0.21
F_{3b}	0.38	0.73	0.35
F_{3c}	0.33	0.66	0.25

* E_{TRANS} = 1.5 eV

   E_{ROT} = 0.08 eV

   Units are 10^{-16} cm^2

TABLE 12. COMPARISON OF MOMENT AND HISTOGRAM CROSS-SECTIONS*

E_{ROT}(eV) Fit	Sudden E_{3a}	0.08 E_{3a}	0.16 E_{3a}	0.40 E_{3a}	0.77 E_{2a}
010					
histogram	0.65	1.7	1.4	2.4	3.4
moment	0.37	0.99	1.3	2.3	2.9
001					
histogram	0.06	0.11	0.22	0.61	0.90
moment	0.13	0.21	0.33	0.58	0.91
100					
histogram	0.22	0.40	0.54	1.0	1.1
moment	0.20	0.31	0.44	0.87	1.0

* E_{TRANS} = 1.5 eV.

  Cross-sections in 10^{-16} cm^2.

This is not the case below 1 eV, at least in part due to the poor statistics for the histogram results, and the moment results are probably more reliable. The moment results are generally found to be reliable only for one-quantum transitions once the histogram probabilities become large. This is not surprising since they are obtained from only the first two moments.

The results in Table 12 also demonstrate the almost linear dependence of the cross sections on initial rotational energy. These results indicate that experimentally determined cross sections will depend on rotational temperature, and that experiments performed using different (perhaps unknown) rotational distributions can yield considerably different cross sections. The sudden results are found in general to be within a factor of two of the 3-D results for $J = 0$.

In Figure 17 excitation cross sections are presented for an initial rotational energy of 0.16 eV, which corresponds to about $J = 10$. The vertical lines through some of the points give 1σ error estimates due to Monte-Carlo sampling. Error estimates for the 011 and 110 cross-sections are seen to overlap. The 020 cross section is not shown, for clarity, since it almost overlaps the 001 cross section from 1-2 eV. The 200 and 002 cross sections are estimated from the moment distributions, and are probably low by a factor of two. Results are presented at 2.5 eV only for the 100 and 010 cross sections, because only 175 trajectories were run and histogram results are not reliable for the other transitions.

65
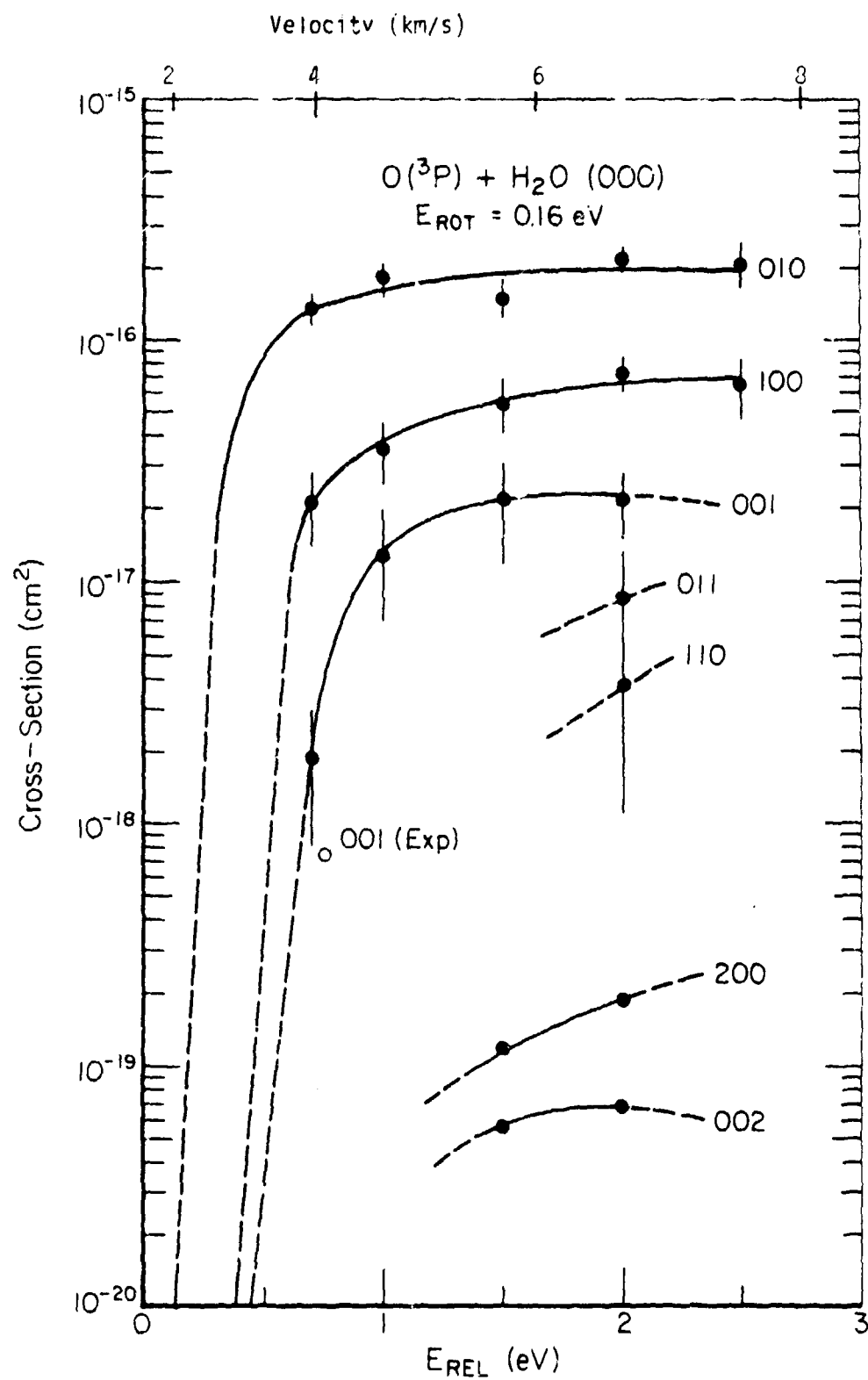
FIGURE 17. CROSS-SECTIONS FOR THE COLLISIONAL
EXCITATION OF H_2O (000) BY $O(^3P)$

Moment cross sections (not shown) track the results reasonably well. For example, at 1.5 eV the moment estimate of the 001 cross section is 1.5 times larger than the histogram result, and for the 010 excitation the histogram result is 1.2 times larger than the moment result. In all cases the moment results are smoother as a function of translational energy.

The experimental point in Figure 17 is the shock-tube result of Dunn and coworkers, Reference 5, for the excitation of the 001 asymmetric stretch. Results of this study for $J = 0$ fall almost through this point, indicating that the experimental conditions must correspond to a low rotational temperature to be consistent with these calculations.

Another observation from the present results is pertinent to the interpretation of the shock-tube and molecular-beam experiments. Since the 100 cross section is greater than the 001 cross section, by about a factor of 4, and since the emissions from the two states overlap, even though the 100 state has a much longer lifetime (180 m sec compared to 17 m sec), the larger 100 cross section might contribute about 40% to the observed signal.

In summary, the results obtained in this study indicate that cross sections for collisional excitation of H_2O by an atomic species can be obtained to within about a factor of two for a given set of ab initio points. This is the conclusion reached by considering different fits to the points as well as two different techniques for generating cross sections.

In summary, the results obtained in this study indicate that cross sections for collisional excitation of H_2O by an atomic species can be obtained to within about a factor of two for a given set of $\underline{ab}$ $\underline{initio}$ points. This is the conclusion reached by considering different fits to the points as well as two different techniques for generating cross sections.

These calculations ignore the possibility of chemical reaction. An attempt was made to assess the importance of excited electronic states by adjusting the sum of pairs fit to correspond with the two excited-state surfaces where points are available. Asymmetric stretch cross sections for the $^3B_2$ state (C_{2v}) are similar to those of the ground state, and cross sections for a model $^3A_2$ surface (C_{2v}) are about 30% larger than the ground state at 2eV. Certainly further work on this system must involve a search for reactive pathways in the potential energy surface. Applications of the surface fitting procedure and the dynamical calculations to a reactive surface would be tedious but tractable.

IV. $O(^3P) + CO_2(^1\Sigma_g^+)$ COLLISION

A. Potential Energy Surface

The collision between $O(^3P)$ and $CO_2(^1\Sigma_g^+)$ differs in several important respects from that observed with H_2O. Primary among these are that the CO bond is much stronger than an OH bond. For example, the stretching force constant for CO_2 is 16 md/$\overset{\circ}{A}$ compared to 8.4 in H_2O. From another viewpoint, it requires more than twice as much energy to break the CO bond as an OH bond. These facts suggest that CO_2 should be harder for an oxygen atom to vibrationally excite than is H_2O. To the contrary, the effective radius of CO_2 is substantially larger than in H_2O. However, this factor contributes only to the elastic cross sections. Since CO_2 is a linear molecule, this surface benefits from higher symmetry than the H_2O case, enabling us to obtain more information from each computed point. Except for approaches along the D_∞ axis, the $O(^3P) + CO_2(^1\Sigma_g^+)$ correlation diagram is similar to that of H_2O. This is illustrated in Figure 18. Figure 19 shows the orientation of CO_2 in the yz plane and the distribution of _ab_ _initio_ points on the surface.

When the oxygen atom approaches along the z-axis (i.e., the D_∞ axis), the possible electronic states are a $^3\Sigma^-$ and a doubly degenerate $^3\Pi$. Just as in H_2O, an approach along the C_2 axis, which is the y-axis in Figure 19, generates the three states, $^3B_1$, $^3B_2$, and $^3A_2$. However, unlike H_2O, when CO_2 is stretched, symmetrically or asymmetrically (but not bent), the values computed at the points indicated on the y-axis define a

FIGURE 18. CORRELATION DIAGRAM FOR DIFFERENT DIRECTIONS OF APPROACH FOR $O(^3P) + CO_2(^1\Sigma_g^+)$
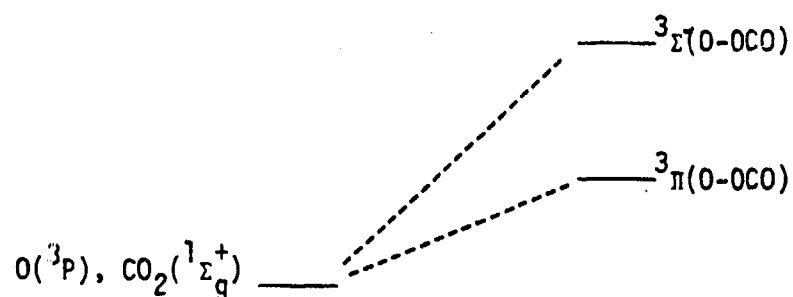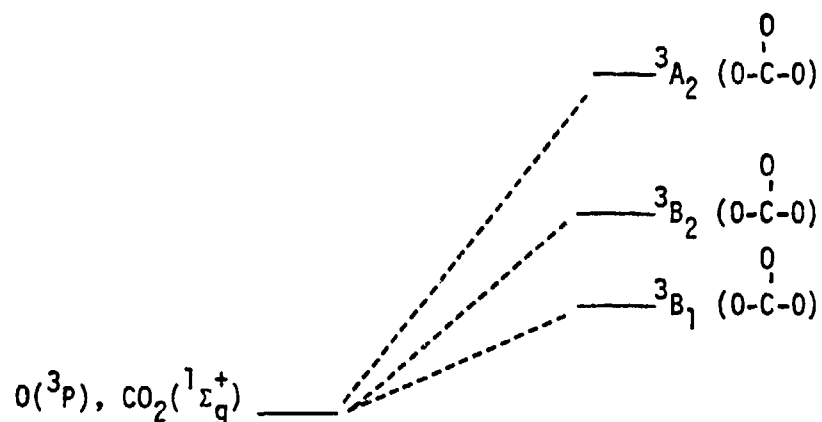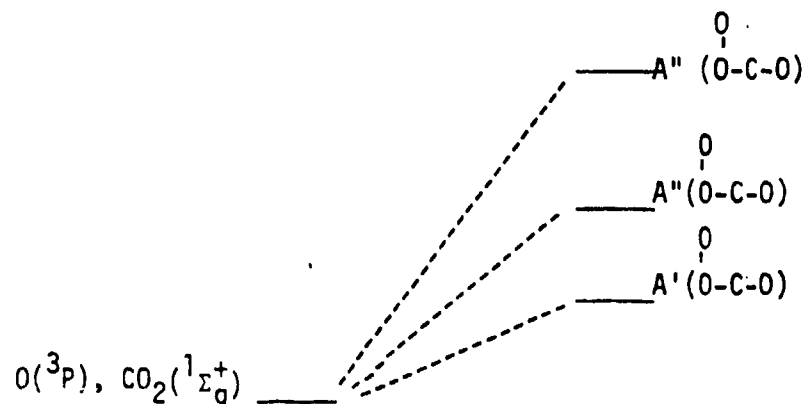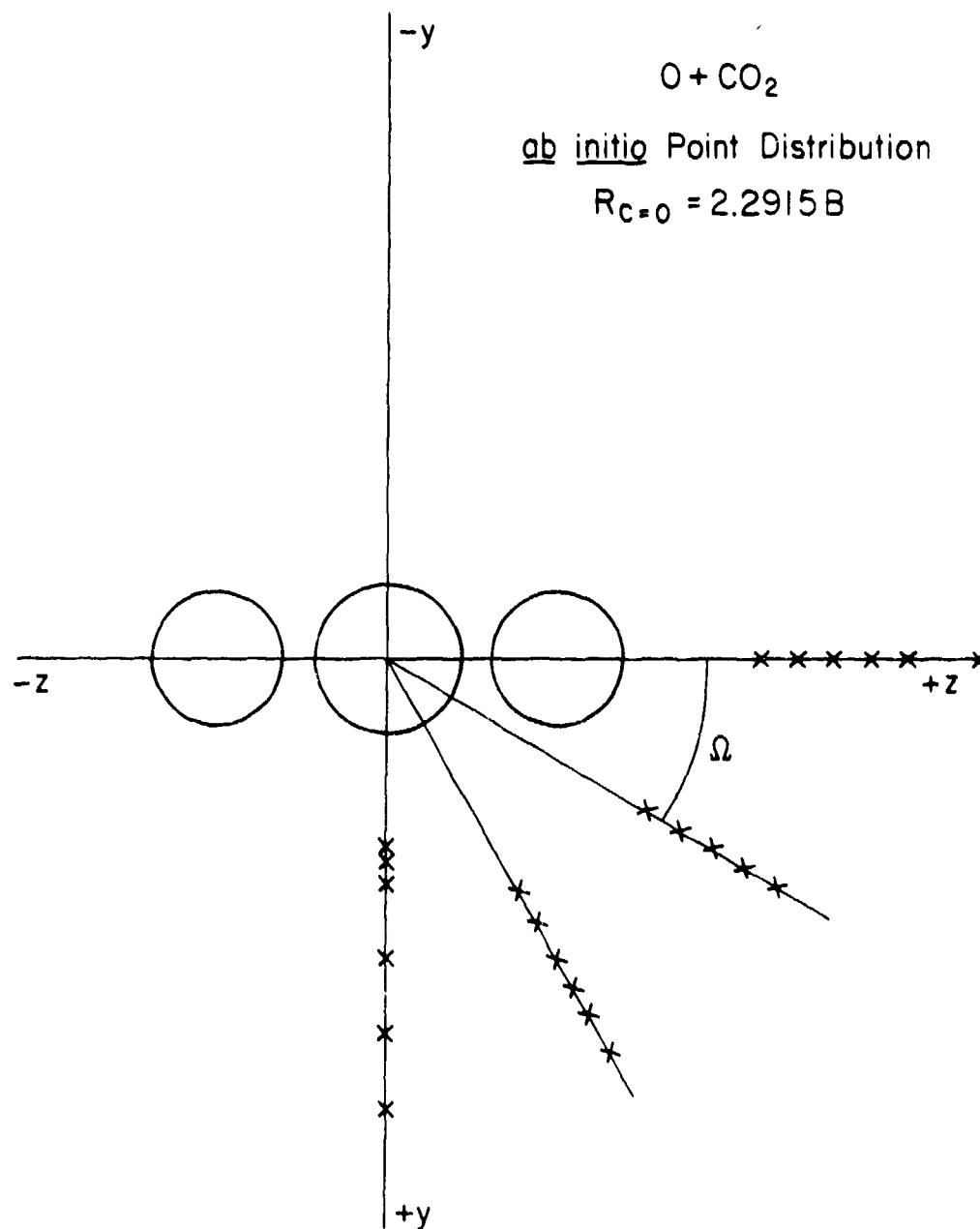
FIGURE 19.   DISTRIBUTION OF AB INITIO POINTS IN THE PLANE
OF THE CO_2 MOLECULE, FOR EQUILIBRIUM CO_2

71

locus of circles about the carbon atom. When a single plane of symmetry is retained, such as by any approach in one of the planes of the CO_2 molecule, the controlling symmetry is C_s, providing a ground A' and two excited A" states.

As justified in our study of the $O(^3P)$ + $H_2O(^1A_1)$ surface, there seems to be little reason to determine the $O(^3P)$ + $CO_2(^1\Sigma_g^+)$ surface using the much more expensive DZP basis set. Consequently, we exclusively employ a double-zeta (DZ) basis in this part of the project. Such a basis is largely incapable of showing much of the very slight Van der Waals region, which should occur about 7-8 bohrs in this system. In the DZP studies of $O(^3P)$ + H_2O, this region is somewhat described, although even a DZP basis is too small to provide an accurate description. However, a fit could introduce the slight Van der Waals well for O + CO_2 from appealing to experiment. In the current studies, this region is found to have such a small effect on the cross sections that it is not considered an important element in the surface in any event. Other than the Van der Waals region, the SDQ-MBPT(4) DZ calculations are found to parallel the DZP calculations on O + H_2O.

The predicted equilibrium structure for CO_2 gives a bond length of 2.2915 bohrs which differs by about 0.08 bohrs from the experimental value. The separated limit is -262.74654 hartrees.

With reference to the distribution of ab initio points for CO_2 at equilibrium, shown in Figure 19, the computed values are presented in Table 16. Figure 20 illustrates the four curves for different angles of approach. Like the H_2O + $O(^3P)$ surface, the repulsive nature of the curves is evident. In H_2O, the surface

72

TABLE 13. $O(^3P) + CO_2$ ($^1\Sigma_g^+$) GROUND STATE SURFACE FOR EQUILIBRIUM CO_2 AS A FUNCTION OF ANGLE OF APPROACH. Ω. ($R_{CO} = 2.2915b$. $\theta_{OCO} = 180°$)

Distance to O-Atom[a] (bohrs)	$\Omega = 0°$(z-axis)		$\Omega = 30°$		$\Omega = 60°$		$\Omega = 90°$(y-axis)	
	SCF	SDQ-MBPT(4)	SCF	SDQ-MBPT(4)	SCF	SDQ-MBPT(4)	SCF	SDQ-MBPT(4)
2.5							-262.12464	-262.54482
3.0							-262.21034	-262.61120
3.5					-262.21031	-262.62338		
4.0			-262.09864	-262.49151	-262.28657	-262.69291	-262.32210	-262.72000
4.5			-262.18394	-262.59554	-262.32323	-262.72562		
5.0	-262.14317	-262.56113	-262.27793	-262.68520	-262.33906	-262.73949	-262.34383	-262.74351
5.5	-262.27784	-262.68272	-262.32229	-262.72463	-262.34533	-262.74481		
6.0	-262.32421	-262.72556	-262.33945	-262.73975	-262.34757	-262.74658	-262.34702	-262.74599
6.5	-262.34069	-262.74073						
7.0	-262.34609	-262.74553						
8.0	-262.34617	-262.74529						
20.0	-262.34762	-262.74654					-262.34762	-262.74654

[a] Distances measured from C-atom in CO_2.

73
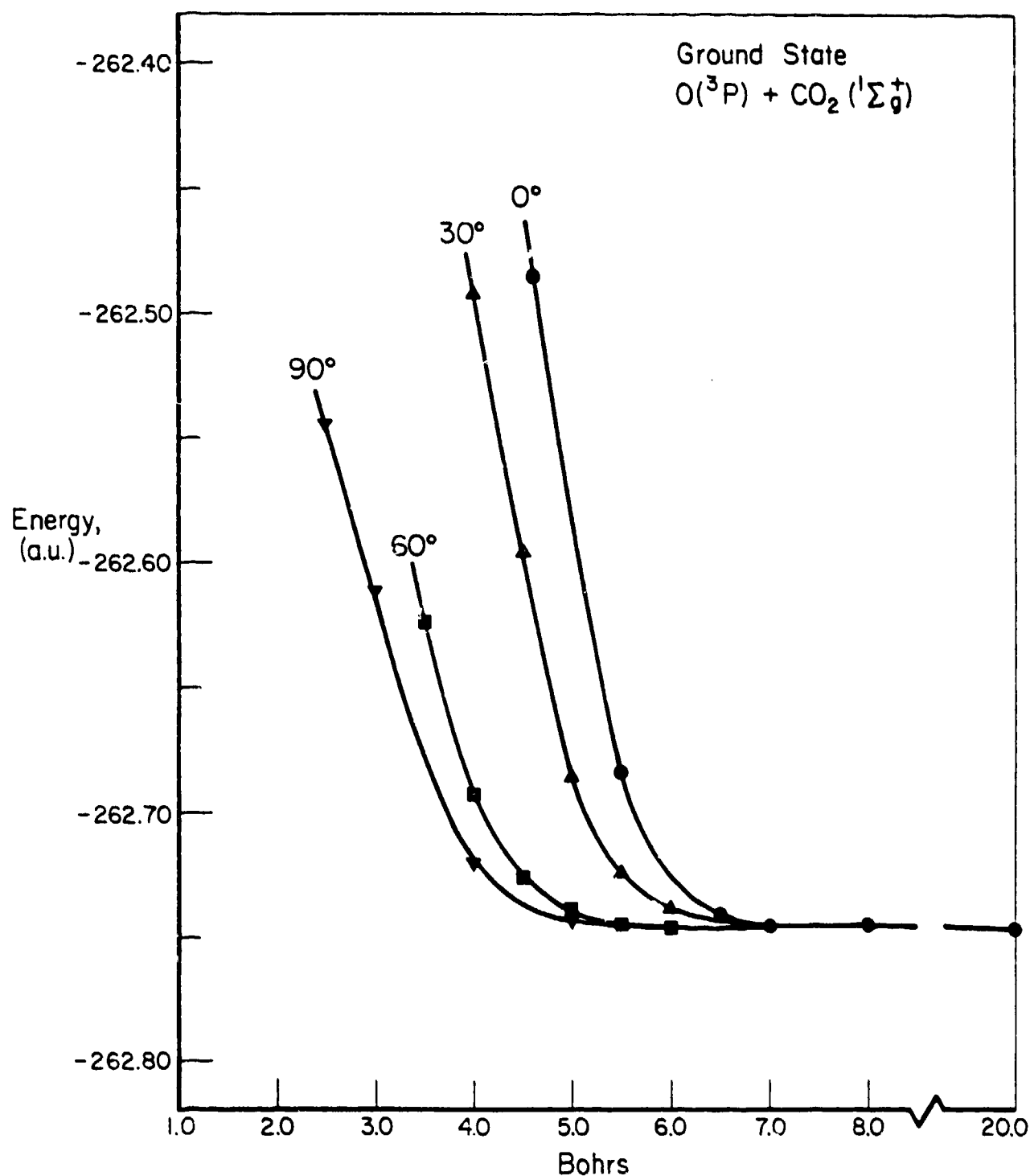
FIGURE 20. COMPARISON OF THE SHAPE OF POTENTIAL SURFACE FOR
$O(^3P) + CO_2$ ($^1\Sigma_g^+$) AS A FUNCTION OF THE ANGLE OF
APPROACH OF O (^3P), WITH CO_2 EQUILIBRIUM

74

is almost spherical, while for CO_2, Figure 18 emphasizes the cylindrical character that one would expect.

The steepest repulsive shoulder corresponds to a collision along the D_∞ axis, rising 0.19 a.u. (i.e., 5eV) from 7 to 5 bohrs. This may be compared with the y-axis approach toward H_2O, illustrated in the bottom curve of Figure 5, which is seen to be less abrupt from 6 to 4 bohrs. This shows that the oxygen atom may approach the smaller molecule more closely, but then increases abruptly by 0.35 a.u. in the one bohr from 3.5 to 2.5 bohrs. Since the H-atoms are displaced from the y-axis in H_2O by about 38°, another pertinent comparison is between the $\Omega = 30°$ curve and Figure 5. In this curve, the approach is less abrupt, changing 0.24 a.u. from 7 to 4 bohrs, compared to almost twice that in H_2O, between 5.5 and 2.5 bohrs. As Ω increases to 90°, the curves are shaped more like those in the H_2O collision, but still remain a little less steep, beginning their ascent in the vicinity of 5 bohrs and rising to 0.2 a.u. in 2.5 bohrs. The slopes of the four curves of Figure 20 in these steep regions are all quite similar.

Through the ability of the oxygen atom to approach H_2O more closely than CO_2, a more drastic increase in the slope occurs, making the H_2O collision harder at short distances, while softer in the intermediate range. The latter is due in some degree to the influence of the dipole moment of H_2O.

In Tables 14 to 16, the computed points for symmetric and asymmetric stretch displacements and a few points for bent CO_2 are reported. For a symmetric displacement the values on the z-axis are

TABLE 14. $C(3P) + CO_2(^1\Sigma_g^+)$ GROUND STATE SURFACE FOR CO_2 IN A SYMMETRIC STRETCH

(R_{CO} = 2.35 b, θ_{OCO} = 180°)

Distance to O-Atom[a] (bohrs)	$\Omega = 0°$ (z-axis)		$\Omega = 30°$		$\Omega = 60°$		$\Omega = 90°$ (y-axis)	
	SCF	SDQ-MBPT(4)	SCF	SDQ-MBPT(4)	SCF	SDQ-MBPT(4)	SCF	SDQ-MBPT(4)
3.0							-262.21615	-262.63877
3.5					-262.20106	-262.62280	-262.27290	-262.67962
4.0					-262.27382	-262.68983		
4.5			-262.17025	-262.58606				
5.0	-262.12817	-262.55613	-262.25993	-262.67761				
5.5	-262.25652	-262.67187						

[a] Distances measured from C-atom in CO_2.

TABLE 15. $O(^3P) + CO_2$ ($^1\Sigma_g^+$) GROUND STATE SURFACE FOR CO_2 IN AN ASYMMETRIC STRETCH MODE. [$O_1(0, 0, -2.33242b)$ $C(0., 0., + 0.10908b)$, $O_2(0., 0., + 2.25060b)$]

	Points[a]			
r	$\theta = \Omega$	ϕ	SCF	SDQ-MBPT(4)
5.5	0.0	90	-262.26705	-262.66806
5.5	180	90	-262.26211	-262.66304
3.5	90	90	-262.26947	-262.66471
4.0	90	90	-262.30853	
4.5	45	90	-262.26587	-262.66962
5.0	45	90	-262.30759	-262.70656
4.5	135	90	-262.26729	-262.67232
5.0	135	90	-262.30822	

[a] Angles $\theta = 45° = 315°$; $\theta = 135° = 225°$; $\theta = 90° = 270°$.

TABLE 16. $O(^3P) + CO_2(^1\Sigma_g^+)$ GROUND STATE SURFACE FOR CO_2 IN A BENT CONFIGURATION [$O_1(O_1, 0.238628b, -2.255210b)$, $C(0., -0.159031b, 0.)$, $O_2(0., 0.238628b, + 2.25521b)$]

	Points			
r	θ	φ	SCF	SDQ-MBPT(4)
2.7	90	90	-262.06239	-262.47364
3.0	90	90	-262.15400	-262.56164
5.3	0	90	-262.23997	-262.64853
5.5	0	90	-262.27269	0262.67856

slightly higher partially reflecting a slight increase in energy due to CO_2 being displaced from its computed equilibrium value, and partially due to the oxygen atom and molecule being somewhat closer. The same trend applies in the case of the 30° and 60° approaches, although at $\Omega = 90°$, the symmetrically displaced terminal atoms serve to slightly facilitate the nearer approach of the oxygen atom.

In the asymmetric case, results are obtained that largely depend upon which side of the molecule is nearest to the colliding oxygen atom. A difference of .005 hartrees is observed on the z-axis at 5.5 bohrs, and somewhat less for the approaches at 45° and 135°, slightly favoring the latter. In the asymetric stretch configuration, the energies on the z-axis are both higher than their values with CO_2 at equilibrium.

Just as in $O(^3P)$, the ground state surface for $O(^3P) + CO_2(^1\Sigma_g^+)$, shows a comparatively simple repulsive nature, which can be conveniently fit to an analytic form as discussed in Section IV. B. The excited states that also correlate with an $O(^3P)$ atom at the separated limit are not considered. In the case of H_2O, these are found to make very little difference in the cross sections. The program plan specifies studying collisions only on the ground state surface; and, because the cross sections obtained in Section IV.D. are so small, a more detailed study incorporating the excited states would be very unlikely to gain more than a factor of 3 or so, while at least an increase of one or two orders of magnitude would be necessary to make the direct excitation of the $CO_2(001)$ mode (as opposed to indirect excitation) an important contributor to the infrared plume signature.

79

B. The Analytical Representation of the
$O(^3P)$ + CO_2 Potential Energy Surface

The PES for $O(^3P)$ + CO_2 is represented in the same general

form as the $O(^3P)$ + H_2O surface, namely as the sum of intramolecular (CO_2)

and intermolecular terms. The intramolecular potential for CO_2 is represented

as a many-body expansion similar to H_2O. There are two significant differences,

however, the first being the use of an experimental CO_2 force field,

rather than a theoretical force field. The second is the use of internal

symmetry coordinates instead of bond displacements for the CO_2 polynomial.

The experimental force field of Kuchitsu and Morino[32] is used since,

unlike H_2O, no theoretical determination of the CO_2 force field of sufficient

accuracy exists.

The form of the CO_2 potential is

$$V_{CO_2}(R_1, R_2, R_3) = V_{CO}(R_1) + V_{CO}(R_3) + V_{O_2}(R_2) + V_3(R_1, R_2, R_3)$$

where R_1 and R_3 are the two C-O bond distances and R_2 is the O-O bond

distance. V_{CO} and V_{O_2} are the $CO(^1\Sigma)$ and $O_2(^3\Sigma_g^-)$ diatomic potentials.

V_3 is a three-body term and has the form

$$V_3 = A(1 - \tanh \gamma_1 S_1^2/2)(1 - \tanh \gamma_2 S_2^2/2)(1 - \tanh \gamma_3 S_3/2)P(S_1, S_2, S_3)$$

where A, γ_1, γ_2, and γ_3 are constants, and P is a polynomial in the

internal coordinates. These are defined as

$$S_1 = (R_3^2 - R_1^2)/(2R_2)$$

$$S_2 = (\frac{1}{2} \tilde{R}_1^2 + \frac{1}{2} R_3^2 - \frac{1}{4} R_2^2 - S_1^2)^{1/2}$$

$$S_3 = R_2 - R_2^0$$

where R_2^0 is the molecular equilibrium value of R_2. Note that V_{CO_2} should be symmetric with respect to $S_1 \rightarrow -S_1$ and $S_2 \rightarrow -S_2$. For this reason the switching functions in V_3 are chosen to be functions of S_1^2 and S_2^2 rather than S_1 and S_2. The use of S_1, S_2, and S_3 rather than R_1, R_2, and R_3, as is done for H_2O, is necessary because the polynomial expansion of V_3 in the latter variables provides an ill-behaved representation of the quartic force field for linear molecules.

The parameters for V_{CO_2} are given in Table 17. In Table 18 the quartic force constants obtained from V_{CO_2} are compared with those of Kuchitsu and Morino, and the agreement is seen to be excellent. The present fit should provide a realistic extrapolation from the accurate representations around equilibrium to the separated diatomic fragments. Figure 21 shows potential contours for stretching displacements of R_1 and R_3.

The $0 + CO_2$ intermolecular potential for the lowest $^3A''$ surface is represented as a sum-of-pairs potential, similar to the E_{2a} fit for H_2O. Time did not permit including higher order terms, but experience with this level of fitting indicates that a reasonable representation of a four-atom nonreactive surface is obtained in this way. Excitation cross

81

$$\text{TABLE 17. PARAMETERS IN } V_{CO_2}{}^{(a)}$$

A. Two Body Terms

$$V_{xy} = -D_{XV}(1 + a_{1xy} \Delta R_{xy} + a_{2xy} \Delta R_{xy}^2 + a_{3xy} \Delta R_{xy}^3)e^{-a_{xy}\Delta R}$$

$$\Delta R_{xy} = R_{xy} - R_{xy}^0$$

$\underline{xy}$	$\underline{D_{XV}}$	$\underline{a_{1xy}}$	$\underline{a_{2xy}}$	$\underline{a_{3xy}}$	R_{xy}^0
CO	11.2245	3.7102	1.5944	1.5422	1.1282
OO	5.2130	5.4454	7.7859	5.9951	1.2078

B. Three Body Terms

$$A = 3.9909$$
$$\gamma_1 = 3.571068$$
$$\gamma_2 = 3.571068$$
$$\gamma_3 = 5.4454$$
$$R_2^0 = 2.32303$$

TABLE 17 . (Continued)

Polynomial Term	Coefficient
1	1
S_3	1.5678
S_1^2	1.5871
S_2^2	2.8483
S_3^2	5.6727
$S_1^2 S_3$	2.8466
$S_2^2 S_3$	3.1655
S_3^3	7.5278
S_1^4	-4.2510
$S_1^2 S_2^2$	3.9974
$S_1^2 S_3^2$	6.8399
S_2^4	3.1893
$S_2^2 S_3^2$	18.391
S_3^4	8.8036

(a) Units are such that unprinted distances in $\overset{\circ}{A}$ give energies in eV.

TABLE 18. QUARTIC FORCE FIELD PARAMETERS
FOR CO_2 POTENTIAL FIT[a]

	Present Fit	Kuchitsu and Morino
ω_1	1354.8	1354.8
ω_2	672.7	673.2
ω_3	2395.7	2395.7
k_{111}	45.0	45.0
k_{122}	-73.9	-73.8
k_{133}	252.5	252.5
k_{1111}	1.2	1.2
k_{3333}	6.6	6.6
k_{1122}	-9.1	-9.1
k_{1133}	20.3	20.3
k_{2233}	-27.7	-27.8

[a] All parameters are in cm^{-1}. For definitions of terms used, see Reference 25.
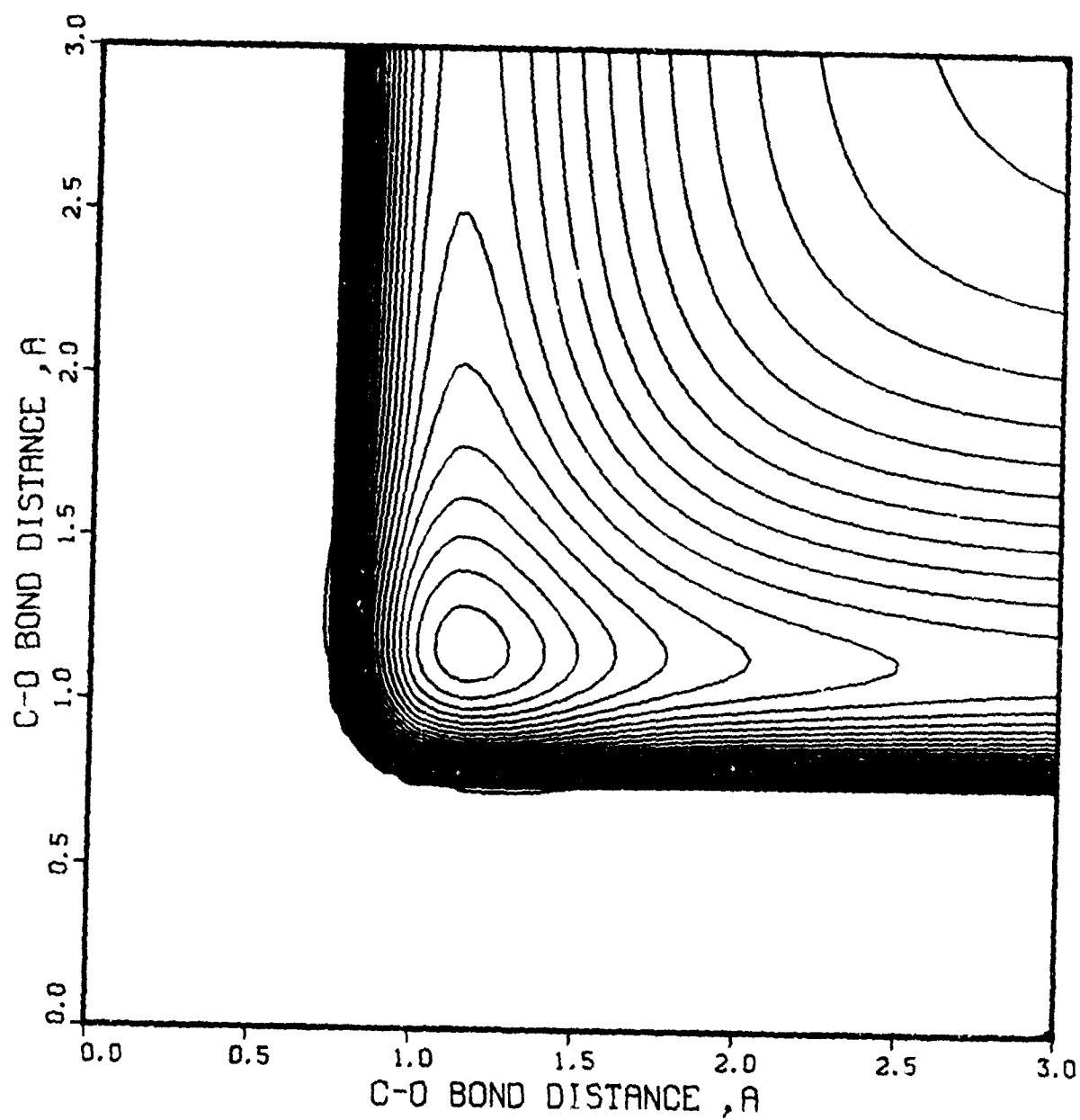
FIGURE 21.   POTENTIAL CONTOURS FOR STRETCHING DISPLACEMENTS
FOR CO_2.   CONTOUR INCREMENT IS 1 eV.

85

sections for $O + H_2O$ on a sum-of-pairs surface differ by no more than a factor of two from cross sections on a more accurate fit containing three-body terms.

Denoting the O atom to C distance as R_4, and the two O atom to O distances as R_5 and R_6, the expression for the intermolecular potential is

$$V_{OCO_2} = Ae^{-\alpha R_4} + Be^{-\beta R_5} + Ce^{-\beta R_6} \quad .$$

The parameters in this expression are $A = 286.97$ eV, $B = 2195.9$ eV, $\alpha = 1.5563 \ a_o^{-1}$, and $\beta = 2.2250 \ a_o^{-1}$.

C. Quasiclassical Trajectory Calculations as Applied to Collisional Excitation of CO_2

Both full 3-D and rotational sudden calculations are made for $O(^3P) + CO_2$ as for $O(^3P) + H_2O$. The procedure for integrating trajectories is similar, but there is one difference in treating the initial and final conditions. For CO_2, an approximation is introduced that involves the omission of a certain Fermi resonant term, one that couples the bend and symmetric stretch modes in the Fourier representation of the good action variables. This term cannot be treated using the presently available nondegenerate perturbation method for defining action-angle variables. Several numerical tests indicate that this term has no influence on excitation of the asymmetric stretch mode. Note that this approximation is only introduced to allow the use of perturbation theory to determine the good actions used in defining quantum states, and that the full interaction potential is used to integrate the trajectories.

As discussed in the application to H_2O, a problem arises with the use of the histogram method in defining state-to-state cross sections when very few or no trajectories finish in the desired bin. This is often true for the CO_2 asymmetric stretch excitation, since rarely more than a few trajectories (out of 1000 to 2000) lead to asymmetric stretch excited states. To extrapolate and interpolate cross sections at velocities where poor statistics make the historgram results unreliable, a moment analysis can be employed, and checked against histogram results where they are available.

In $0 + H_2O$, an exponential expression is found to conveniently represent the final state distributions. In the case of $0 + CO_2$, this is not as satisfactory, but an expression

$$0 \ \alpha \ <\Delta N_3^2>^X$$

seems to be suitable. The value $X = 1.3$ accurately represents the nonzero histogram results and is consequently used to determine the interpolated cross sections.

D. Cross Sections for Collisional Excitation of CO_2 by $O(^3P)$ Atom Impact

Figure 22 and Table 19 presents the theoretical cross sections for excitation of the asymmetric stretch mode of CO_2. The result labelled Q(001) is for the direct process 000→001, while the label Q(NN̂1) results from summation over the symmetric stretch quantum number N and the bend quantum Number N for those transitions leading to one quantum of excitation in the asymmetric stretch mode. Since infrared fluorescence between (NN'1) combination states and (NN̂ 0) significantly overlap the 001→000 emission, it is likely that many experiments are actually measuring the total cross section Q(NN̂1) rather than Q(001). At velocities of 6 km/sec or greater, this study shows that combination state excitation is substantially more probable than direct excitation of the 001 state, so that Q(NN̂ 1) is much larger than Q(001).

The results in Table 19 suggest that Q(001) is immeasurably small except at very high velocities. At 6 km/sec, Q(001) has a value from this study of 3×10^{-20} cm^2, while Q(NN'1) has a much larger value of 1×10^{-18} cm^2. Statistical uncertainty in these results is $\pm$ 50 percent.

The effects of CO_2 rotational excitation on both Q(001) and Q(NN'1) are summarized in Table 20. A slow increase in these cross sections with increasing J is found up to high rotational energy. Although this result is different than found for $O + H_2O$, it is consistent with the greater time scale separation between rotation and vibration in CO_2 relative to H_2O due to the large CO_2 moment of inertia.
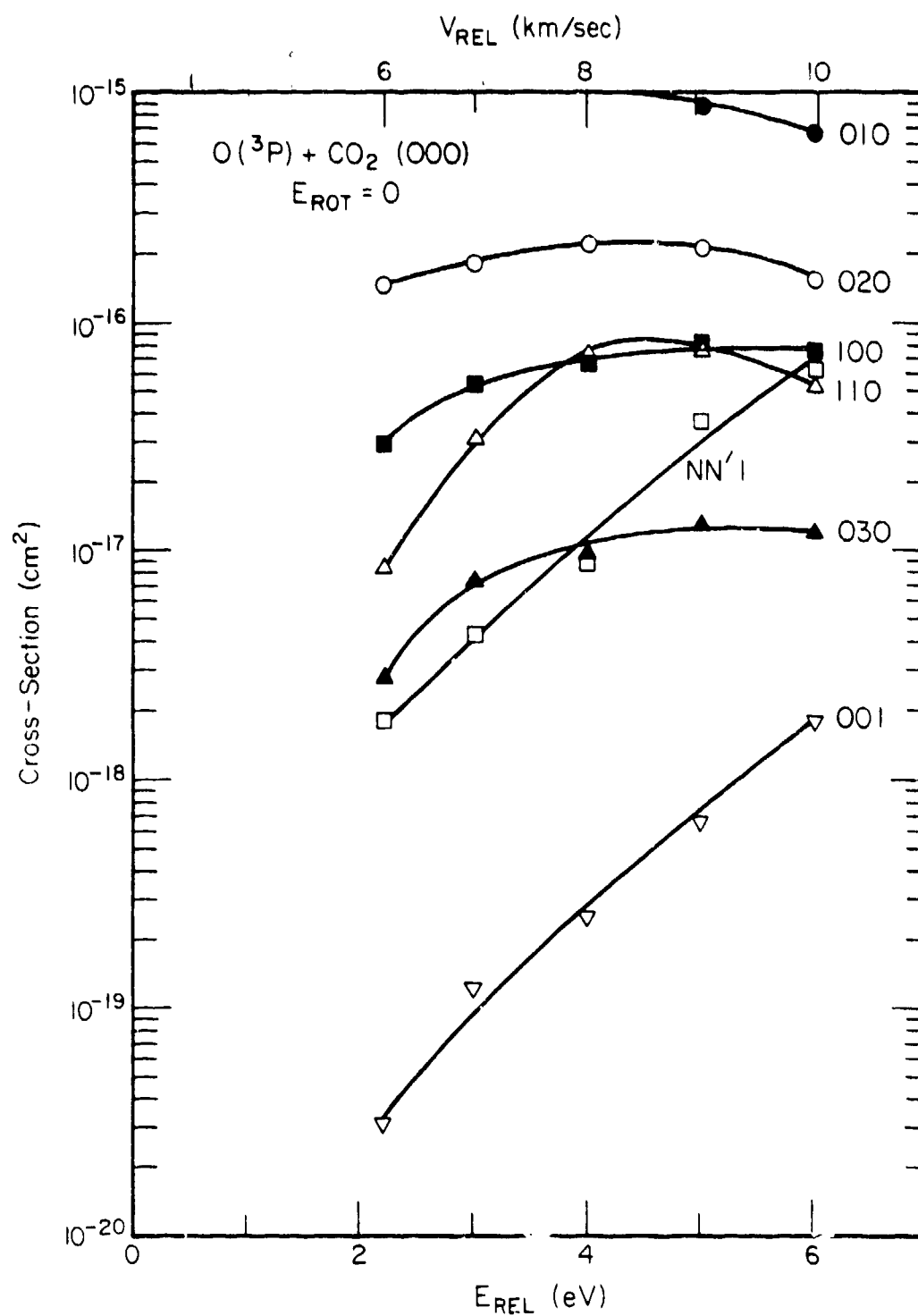
FIGURE 22. CROSS-SECTIONS FOR THE COLLISIONAL EXCITATION OF CO_2 (000)

TABLE 19. TRAJECTORY INTEGRATION PARAMETERS AND INTEGRAL CROSS SECTIONS FOR $O + CO_2$

$E_0^a(eV) =$	2.2	3.0	4.0	5.0	6.0
$v^b(km/sec)$	6.0	7.0	8.1	9.1	9.9
No. trajectories	300	1000	2000	2000	1000
Max. l.	450	500	550	650	750
$\langle \Delta N_1^2 \rangle^c$	0.043	0.060	0.121	0.220	0.366
$\langle \Delta N_2^2 \rangle^d$	0.584	0.803	1.513	2.410	3.308
$\langle \Delta N_3^2 \rangle^e$	0.00115	0.00305	0.00532	0.0113	0.0240
$Q(001)^f$	3×10^{-20}	1.2×10^{-19}	2.5×10^{-19h}	6.7×10^{-19}	1.8×10^{-18h}
$Q(NN'1)^g$	1×10^{-18}	4.3×10^{-18}	8.8×10^{-18h}	3.7×10^{-17h}	6.3×10^{-17h}

a Initial translational energy.
b Initial relative velocity.
c Symmetric stretch action second moment.
d Bend action second moment.
e Asymmetric stretch action second moment.
f $000 \rightarrow 001$ cross section in cm^2.
g $000 \rightarrow NN'1$ cross section, summed over all N,N' for which $V_3 = 1$.
h This denotes cross section obtained directly from the histogram method. All others were obtained from the scaling formula.

91

TABLE 20.   EFFECT OF CO_2 ROTATION ON VIBRATIONAL
EXCITATION CROSS SECTIONS[a]

E_{ROT}(eV)	0	.025	.087
$J(CO_2)$	0	23	42
No. trajectories	2000	1000	1000
MAX ℓ	550	550	550
Q(001)	2.5×10^{-19}	2.8×10^{-19}[b]	3.9×10^{-19}[b]
Q(NN'1)	8.8×10^{-18}	1.0×10^{-17}[b]	1.4×10^{-17}[b]

[a] Cross sections are in cm^2.   Relative velocity is 8.1 km/sec.

[b] Result of scaling calculation.   Where histogram values were also
obtained, the scaling result agrees with the histogram result
within the statistical uncertainty of the latter.

V. DISCUSSION OF RESULTS AND SUGGESTIONS FOR FURTHER WORK

This report presents results of a first-principle theoretical determination of cross sections for vibrational excitation of H_2O and CO_2 from collisions with $O(^3P)$ atoms. Correlated potential energy surfaces are obtained with many-body perturbation theory and fit to analytical expressions. The analytical fits are used in quasiclassical trajectory calculations to determine vibrational excitation cross sections averaged over final rotational states. Classical perturbation theory is used to solve the Hamilton-Jacobi equations to obtain good actions for the semi-classical final state analysis.

A goal in this work is the prediction of cross sections to within a "factor of two" of their accurate values. To this end the effects of errors in the results due to approximations in each phase of the calculation are investigated by running trajectories on various fits to the potential surfaces. This procedure uses fits that differ from one another by more than the errors in an ab initio surface, and also fits that reflect the differences between the ground state surface and the first two excited states for H_2O. In most cases the cross sections are changed by less than a factor of two. One exception occurs when a quartic force field is used for the H_2O potential, in which case the cross sections differ from a more realistic fit by an order of magnitude. Convergence to the correct potential is assured by comparisons of different levels of correlation and by using different basis sets.

Theoretical studies such as this are not only of value because of the large number of excitations for which results are obtained, but as an aid to the experimentalist as well. In addition to providing results for transitions that cannot be determined by experiment, results often can help in the interpretation of the experiments. The dependence of the cross sections on rotational energy discussed in the text indicates that reagent rotational temperature will affect the vibrational energy transfer. This might be important in interpreting shock-tube results. Also a larger cross section for 100 than 001 in H_2O can affect the experimental interpretation.

The results for CO_2 show that excitation of NN1 states is more probable by up to two orders of magnitude than direct excitation of the 001 state. As discussed in the text, radiation from NN1 states is likely to obscure the 001 radiation, and this can affect cross sections obtained in some experiments. If radiation from 001 is indeed observed, then a multiple collision environment probably exists and a study of collisional deactivation of excited vibrational states to 001 is necessary. It should be noted that final state rotational distributions and angular distributions can be obtained from the theoretical approach, and would likely lead to an increased understanding of these collision processes.

Just as there are many difficulties in complex beam and shock tube experiments, there are characteristic problems in the theoretical calculations as well. These problems are discussed more fully throughout this report, but it is useful to summarize the possible errors here in order to assess the reliability of the computed results and to suggest possible future refinements of the calculations.

Initially, it should be emphasized that all results reported here are first principle, except that empirical information is used for the CO_2 force field. The information with which we start is simply the nuclear charges and the numbers of electrons of the atoms involved. The electrostatic hamiltonian constructed from this information includes the kinetic energy of the electrons, the electron-nuclear attraction, and the interelectron repulsions. Armed with such a hamiltonian we attempt to solve Schrödinger's equation to define the PES.

The method of solution is approximate in the sense that a finite number of basis functions are used and all possible interelectronic repulsive effects (called correlation) are not included. However, demonstrated experience tells us that the level at which we are solving Schrödinger's equation is sufficient for the problem at hand. We also find only insignificant differences in the PES when changing from a small number of basis functions (i.e., the double-zeta level, DZ) to a larger number (i.e., double-zeta plust polarization, DZP). Similarly, only small changes occur between the uncorrelated self-consistent field results and our SDQ-MBPT(4) model, which essentially adds all the correlation effects due to single-, double-, and quadruple-excitations into the problem. This tells us that an improvement in basis set or in a higher inclusion of correlation effects is not going to make any important difference in the PES, so Schrödinger's equation is essentially solved for the ground state PES.

The next stage of the calculation involves the analytic fit to the computed $\underline{ab}$ $\underline{initio}$ points whose accuracy seems sufficient. The accuracy of the cross sections is therefore primarily a function of the quality of the fit to the computed points. If the fit is good most places, but introduces wells or barriers that should not be present, cross sections could be inaccurate. This is a difficult part of the problem because as yet, there is no general procedure for fitting a four-atom surface.

As a result there are many approaches, and building upon one of these that has been found to be successful, a satisfactory procedure has been developed during the co_rse of this work. We have been greatly helped in this by the simple repulsive nature of the computed surfaces. About the only test of the fit that is possible, other than simply making several plots that compare the fit to the computed points, is to attempt some "sensitivity" analysis. Essentially, this means compute the cross-sections from trajectory calculations for a given fit to the surface, then modify several of the parameters in the fit and repeat the cross section calculations. If this is done for a fairly wide range of possible fitting parameters, it is possible to conclude that the cross-sections change within a specified tolerance. This is done for the H_2O cross sections, concluding that the cross sections are insensitive to within a factor of 2 for substantial changes in the fit parameters. This provides a measurable degree of confidence in the predicted results. Due to the use of a simpler fit for the $O + CO_2$ surface, the cross sections are not as reliable as for $O + H_2O$. Future work should involve obtaining a better fit.

The last element in the computation, the actual determination
of the cross sections, also involves approximations. Recognizing that
the collision velocities of interest in this work are relatively high,
it is possible to use quasiclassical trajectory methods to obtain the
cross sections. This means using classical mechanics to describe the
actual colliding particles, but combining these techniques with good
action-angle variables that permit the trajectories to be reliably
resolved into specified vibrational-rotational states. When the number
of trajectories binned into a vibrational-rotational state is statisti-
cally inadequate, then either an exorbitant number of trajectories must
be computed to obtain statistically meaningful results, at great expense,
or the histogram method needs to be augmented with moment analysis, as
described in this report. The application of moment methods to polyatomics
is new with this work, and its reliability for different types of excitation
has not been investigated. Care is taken in this study to obtain pro-
cedures that are reliable for the asymmetric stretch excitations.

Since there are many possible rotational states for each
vibration, several thousand trajectories would be required for statistically
meaningful results for rotational distributions. The objective of this
work, instead, is to provide vibrational cross sections averaged over
the rotational states. For the case of a very small collision-induced
vibrational excitation, such as the (001) cross section in CO_2, statistical
uncertainties can be high, but recognizing the small magnitude of these
quantities is sufficient to discount the importance of direct excitation
of this state in the plume signature.

97

The other approximation in the actual cross section determination involves the perturbation approach, required for efficiency, that is used to resolve the trajectories into the various quantum states. For very high internal excitation, the perturbation theory does not converge. Also, when the amount of rotational energy is equivalent to vibrational excitation, coriolis coupling tends to produce large temporal oscillations in the actions. These problems do not affect the present results.

This discussion describes some of the significant approximations made in this work, all of which we believe are sufficiently accurate for this study. However, there are other approximations which are more difficult to discount without additional work. Since all of these are outside the scope of the current project, and since they mostly pertain to higher-order effects on the cross sections, they have only been considered superficially. A more thorough investigation is warranted.

Since an $O(^3P)$ atom colliding with a molecule in a totally symmetric ground state produces three electronic PES, the cross sections for the collision are a function of all these states. One computes a cross section for each possible electronic PES, and the total, observed state-to-state cross sections are found as one-third of the sum of the cross sections. The difficulty and expense of determining these PES requires that this first effort should essentially focus only on the ground state as it does, although in H_2O, the excited states are also considered to some degree. When all three states are determined, the two lowest are found to be quite similar, with the third somewhat more repulsive. By adjusting the fit of the surface to account for the

changes in shape in the excited surfaces, an estimate of the change in the cross section due to excited states is made, and found to be on the order of 30 percent for H_2O.

In CO_2, only the ground surface is considered. If there are larger changes among the three states than anticipated, different, probably somewhat larger cross sections would be found. A thorough study of these excited state PES would require an approach for solving Schrödinger's equation that gives excited states of the same symmetry as the lower states. We are developing many-body approaches for this problem, CI approaches are applicable, and some MC-SCF techniques, but this is still a difficult problem. Indirect pathways for producing 4.3 μ radiation, probably involving multiple collisions, should also be investigated

Another area for a more thorough investigation pertains to the possible reactive channel in $O(^3P) + H_2O(^1A_1) \rightarrow 2OH(^2\pi)$. To study this, we must focus on the reactive region of the energy surface and locate a transition state. It appears from the correlation diagram, that the $OH(^2\cdot)$ molecule can be formed on both the ground and first excited PES, again placing emphasis on a knowledge of the excited state. The sign of any possible error due to this approximation is hard to assess. The effect of reaction on the nonreactive flux could be estimated if the properties of the transition state were known. The more reaction actually occurs, the less flux will enter the vibrational excitation channels, reducing the cross sections. However, if the surface develops a pathway leading to these products, it may also enhance the vibrational cross sections by providing

an area that would encourage repeated collisions. Also, the possible infrared emission of OH itself could also contribute importantly to the plume signature, and this should be investigated for that reason as well.

A third area for future research would be to study the $O(^3P)$ + HF and $O(^3P)$ + HCl collisions. These should have most of the same properties already observed for H_2O and CO_2, but may add some new features since HOF, HFO, etc., probably have a degree of stability. The PES for these surfaces are easier to obtain precisely because they have only three degrees of freedom, compared to six for the H_2O and CO_2 collisions. Again, the experiments are highly difficult for these systems, and reliable calculations should be a cost effective approach to obtaining the necessary kinetic data.

A fourth direction for additional work would be the H_2O with H_2O collision. This seems to be an important contributor to plume signatures. Since it involves 12 degrees of freedom, and one can compute only a limited number of points on the surface, the behavior of the analytic fit to this surface would have to account for much more of the shape of the surface than in the O + H_2O or CO_2 collisions. However, we have an exceptional fit for H_2O itself which could be incorporated into the six-atom surface. In addition, there is only a single PES for H_2O + H_2O and no open-shells are involved to complicate the calculations. The H_2O + H_2O surface would have a number of local minima that the fit would need to correctly describe.

One other problem worth mentioning is the collision of N_2 with H_2O and CO_2. Again, there is only a single PES for their closed-shell molecules, and there is quite a bit of experimental information on this system. It would be interesting to study these collisions as a function of vibrational/rotational state for N_2.

In the area of plume identification and detection, many other possibilities for future theoretical calculations exist, since much of the resolution of the signature problem rests upon a detailed knowledge of the atom-atom, atom-molecule, and molecule-molecule interactions. First principle theoretical chemistry can contribute significantly to all of these problems.

REFERENCES

1. J. S. Draper, J. A. Sutton, "J. Spacecraft and Rockets 10, 10 (1973).

2. C. E. Kolb, M. Camac, R. B. Subbaro and T. B. Anderson, "Experimental Studies of the Collisional Excitation of Infrared Active Vibrational Stretch Modes in CO_2 and H_2O With an Intersecting, Hyperthermal Molecular Beam Apperatus" AFRPL-TR-75-2.

3. T. J. Rieger, K. S. Tait, and H. R. Baum, J. Quant. Spectrosc. Radiat. Transfer 15, 1117 (1975).

4. C. E. Kolb, "Experimental Studies of the Collisional Excitation Stretch Modes in CO_2 and H_2O With an Intersection Hyperthermal Molecular Beam Apparatus," NTIS, AP/A-006-237 (1975).

5. M. G. Dunn, G. T. Skinner, and C. E. Treanor, "Infrared Radiation From H_2O, CO_2, or NH_3 Collisionally Excited by N_2, O, or Ar," AIAA Journal 13, 803 (1975).

6. R. J. Bartlett and G. D. Purvis, III, "Molecular Applications of Coupled-Cluster and Many-Body Perturbation Methods," Physical Scripta 21, 255 (1980).

7. R. J. Bartlett, G. D. Purvis, III "Many-Body Perturbation Theory, Coupled-Pair Many-Electron Theory, and the Importance of Quadruple Excitations for the correlation Problem," Int. J. Quatum Chem. 14, 561 (1978).

8. R. J. Bartlett, I. Shavitt, and G. D. Purvis, III, The Quartic Force Field of H_2O Determined by Many-Body Methods that include Quadruple Excitation Effects," J. Chem. Phys. 71, 281 (1979).

9. G. F. Adams, G. D. Bent, G. D. Purvis, III, and R. Bartlett, "Calculation of Dissociation Energies Using Many-Body Perturbation Theory," Chem. Phys. Letter., in press.

10. L. T. Redmon, G. D. Purvis, III, and R. J. Bartle, "Accurate Binding Energies of Diborane, Borane Carbonyl, and Boraza are determined by Many-Body Perturbation Theory," J. Am. Chem. Soc., 2856 (1979).

11. L. T. Redmon, G. D. Purvis, III, and R. J. Bartle, "Correlation Effects in the Isomeric Cyanides: HNC HCN, LiNC LiNC, and BNC BCN," J. Chem. Isocyanide to Methyl Cyanide," J. Chem. P 72, 986 (1980); Isomerization of Methyl Isocyanide to Methyl Cyanide Acetonitrile) J. Chm. Phys. 69, 5386 (1978).

12. G. F. Adams, G. D. Bent, G. D. Purvis, III, and R. J. Bartlett, "The Electronic Structure of the Formyl Radical, HCO," J. Chem. Phys. $\underline{71}$, 3699 (1979)

13. B. A. Brandow, "Linked-Cluster Expansions for the Nuclear Many-Body Problem," Rev. Mod. Phys. $\underline{39}$, 771 (1967).

14. I. Lindgren, "A Coupled-Cluster Approach to the Many-Body Perturbation Theory for Open-Shell Systems," Int. J. Quantum Chem. Symp. $\underline{12}$, 33 (1978).

15. L. M. Raff, L. Stivers, R. N. Porter, D. L. Thompson, and L. B. Sims, "Semiempirical VB Calculations of the (H_2, I_2) Interaction Potential," J. Chem. Phys. $\underline{52}$, 3449 (1970).

16. L. M. Raff, "Theoretical Investigations of the Reaction Dynamics of Polyatomic Systems: Chemistry of the Hot Atom $(T^* + CH_4)$ and $(T^* + CD_4)$ Systems," J. Chem. Phys. $\underline{60}$, 2220 (1974).

17. J. C. Tully, "Diatomics-in-Molecules Potential Energy Surfaces. I. First-Row Triatomic Hydrides," J. Chem. Phys. $\underline{58}$, 1396 (1973).

18. S. Carter, I. M. Mills, and J. N. Murrell, "A Potential Energy Surface for the Ground State of Formaldehyde, H_2CO (X^1A_1)," Mol. Phys. $\underline{39}$, 455 (1980).

19. D. R. McLaughlin and D. L. Thompson, "Ab Initio Dynamics: $H_3H^+ + H_2 \to HC + H_3^+$ (C_{2v}) Classical Trajectories Using a Quantum Mechanical Potential Energy Surface," J. Chem. Phys. $\underline{59}$, 4393 (1973).

20. N. Sathyamunthl and L. M. Raff, "Quasiclassical Trajectory Studies Using 3D Spline Interpolation of Ab Initio Surfaces," J. Chem. Phys. $\underline{63}$, 464 (1975).

21. J. W. Downing, J. Michl, Jiri Cizek, and J. Paldus, "Multidimensional Interpolation by Polynomial Roots," Chem. Phys. Lett. $\underline{67}$, 377 (1979).

22. A.J.C. Varandas and J. N. Murrell, "A Many-Body Expansion of Polyatomic Potential Energy Surfaces: Applications to H_n Systems," J. Chem. Soc., Faraday II, $\underline{73}$, 939 (1977).

23. R. L. Vance and G. A. Gallup, "Representation of Ab Initio Energy Surfaces by Analytic Functions," J. Chem. Phys. $\underline{69}$, 736 (1978).

24. K. S. Sorbie and J. N. Murrell, "Analytical Potentials for Triatomic Molecules from Spectroscopic Data," Mol. Phys. $\underline{29}$, 1387 (1975).

25. M. J. Redmon and G. C. Schatz, "An Analytical Fit to an Accurate Ab Initio ($^1A_1$) Potential Surface for H_2O," to appear in Chemical Physics.

26. A review on this topic is: D. G. Truhlar and J. T. Muckerman, "Reactive Scattering Cross Sections II: Quasiclassical and Semiclassical Methods in Atom Molecule Collision Theory, A Guide for the Experimentalist," R. B. Bernstein, ed. (Plenum, New York, 1979), Chapter 6.

27. A review on this topic is: I. C. Perceival, "Semiclassical Theory of Bound States," Adv. Chem. Phys. 36, 1 (1977).

28. G. C. Schatz and T. Mulloney, "Classical Perturbation Theory of Good Action-Angle Variables. Applications to Semiclassical Eigenvalues and to Collisional Energy Transfer in Polyatomic Molecules," J. Phys. Chem. 83, 989 (1979).

29. G. C. Schatz and H. Elgersma, "A Quasiclassical Trajectory Study of Product Vibrational Distributions in the OH + H_2 → H_2O + H Reaction," Chem. Phys. Lett 73, 21 (1980).

30. T. Mulloney and G. C. Schatz, "Classical Rotational and Centrifugal Sudden Approximations for Atom-Molecule Collisional Energy Transfer," Chem. Phys. 45, 213 (1980).

31. G. C. Schatz, "A Quasiclassical Trajectory Study of Collisional Excitation in Li^+ + CO_2," J. Chem. Phys. 72, 3929 (1980).

32. K. Kuchitsu and Y. Morino, "Estimation of Anharmonic Potential Constants. I. Linear XY_2 Molecules" Bulletin of the Chemical Society of Japan, 38, 805 (1965).